# STRUCTURE AND FORMATION OF cD GALAXIES: NGC 6166 IN ABELL 2199

| | |
|---|---|
| **Citation** | Bender, Ralf, John Kormendy, Mark E. Cornell, and David B. Fisher. "STRUCTURE AND FORMATION OF cD GALAXIES: NGC 6166 IN ABELL 2199." The Astrophysical Journal 807, no. 1 (June 30, 2015): 56. © 2015 The American Astronomical Society |
| **As Published** | http://dx.doi.org/10.1088/0004-637X/807/1/56 |
| **Publisher** | IOP Publishing |
| **Version** | Final published version |
| **Citable link** | http://hdl.handle.net/1721.1/98309 |
| **Terms of Use** | Article is made available in accordance with the publisher's policy and may be subject to US copyright law. Please refer to the publisher's site for terms of use. |

# STRUCTURE AND FORMATION OF cD GALAXIES: NGC 6166 IN ABELL 2199*

Ralf Bender[1,2], John Kormendy[1,2,3], Mark E. Cornell[3,4], and David B. Fisher[3,5]

[1] Max-Planck-Institut für Extraterrestrische Physik, Giessenbachstrasse, D-85748 Garching-bei-München, Germany; bender@mpe.mpg.de
[2] Universitäts-Sternwarte der Ludwig-Maximilians-Universität, Scheinerstrasse 1, München D-81679, Germany
[3] Department of Astronomy, University of Texas at Austin, 2515 Speedway, Stop C1400, Austin, TX 78712-1205, USA; kormendy@astro.as.utexas.edu
[4] MIT Lincoln Laboratory, ETS Field Site, P.O. Box 1707, Socorro, NM 87801, USA; Mark.Cornell@ll.mit.edu
[5] Centre for Astrophysics and Supercomputing, Swinburne University of Technology, Mail Stop H30, P.O. Box 218, Hawthorn, Victoria 3122, Australia; dfisher@astro.swin.edu.au
Received 2014 November 10; accepted 2015 May 1; published 2015 June 30

## ABSTRACT

Hobby–Eberly Telescope (HET) spectroscopy is used to measure the velocity dispersion profile of the nearest prototypical cD galaxy, NGC 6166 in the cluster Abell 2199. We also present composite surface photometry from many telescopes. We confirm the defining feature of a cD galaxy; i.e., (we suggest), a halo of stars that fills the cluster center and that is controlled dynamically by cluster gravity, not by the central galaxy. Our HET spectroscopy shows that the velocity dispersion of NGC 6166 rises from $\sigma \simeq 300 \, \mathrm{km \, s^{-1}}$ in the inner $r \sim 10''$ to $\sigma = 865 \pm 58 \, \mathrm{km \, s^{-1}}$ at $r \sim 100''$ in the cD halo. This extends published observations of an outward $\sigma$ increase and shows for the first time that $\sigma$ rises all the way to the cluster velocity dispersion of $819 \pm 32 \, \mathrm{km \, s^{-1}}$. We also observe that the main body of NGC 6166 moves at $+206 \pm 39 \, \mathrm{km \, s^{-1}}$ with respect to the cluster mean velocity, but the velocity of the inner cD halo is $\sim 70 \, \mathrm{km \, s^{-1}}$ closer to the cluster velocity. These results support our picture that cD halos consist of stars that were stripped from individual cluster galaxies by fast tidal encounters.

However, our photometry does not confirm the widespread view that cD halos are identifiable as an extra, low-surface-brightness component that is photometrically distinct from the inner, steep-Sérsic-function main body of an otherwise-normal giant elliptical galaxy. Instead, all of the brightness profile of NGC 6166 outside its core is described to $\pm 0.037 \, V \, \mathrm{mag \, arcsec^{-2}}$ by a single Sérsic function with index $n \simeq 8.3$. The cD halo is not recognizable from photometry alone. This blurs the distinction between cluster-dominated cD halos and the similarly-large-Sérsic-index halos of giant, core-boxy-nonrotating ellipticals. These halos are believed to be accreted onto compact, high-redshift progenitors ("red nuggets") by large numbers of minor mergers. They belong dynamically to their central galaxies. Still, cDs and core-boxy-nonrotating Es may be more similar than we think: both may have outer halos made largely via minor mergers and the accumulation of tidal debris.

We construct a main-body+cD-halo decomposition that fits both the brightness and dispersion profiles. To fit $\sigma(r)$, we need to force the component Sérsic indices to be smaller than a minimum-$\chi^2$ photometric decomposition would suggest. The main body has $M_V \simeq -22.8 \simeq 30\%$ of the total galaxy light. The cD halo has $M_V \simeq -23.7$, $\sim 1/2$ mag brighter than the brightest galaxy in the Virgo cluster. A mass model based on published cluster dynamics and X-ray observations fits our observations if the tangential dispersion is larger than the radial dispersion at $r \simeq 20''$–$60''$. The cD halo is as enhanced in $\alpha$ element abundances as the main body of NGC 6166. Quenching of star formation in $\lesssim 1$ Gyr suggests that the center of Abell 2199 has been special for a long time during which dynamical evolution has liberated a large mass of now-intracluster stars.

*Key words:* galaxies: elliptical and lenticular, cD – galaxies: evolution – galaxies: formation – galaxies: kinematics and dynamics – galaxies: photometry – galaxies: structure

## 1. INTRODUCTION

Matthews et al. (1964) and Morgan & Lesh (1965) introduced the cD class[6] of galaxies in the context of the

---

[6] The name "cD" has created some confusion. It has been interpreted to mean "cluster dominant" or "central dominant" or "central diffuse." All are correct descriptions, but they are not the origin of the name. Morgan (1958) introduced the "D" form classification for galaxies that are like ellipticals but with distinct, outer halos with shallow brightness gradients. The "D" class has not been as useful as Hubble classes (Hubble 1936; Sandage 1961), because it includes several different physical phenomena, (a) S0 galaxies, in which the outer halo is the disk; (b) giant ellipticals with high Sérsic (1968) indices $n \gg 4$, and (c) the subjects of this paper: giant ellipticals whose distinct outer halos consist of intracluster stars that have been stripped from cluster galaxies. Because this involves important physics, the name "cD" has survived even though the name "D" has not. But "c" does not mean "central" or "cluster." Rather, it is a historical anachronism that survives from stellar spectral classes that are no longer used. Quoting Matthews et al. (1964): "These very large D galaxies observed in clusters are given the prefix "c" in a manner similar to the notation for supergiant stars in stellar spectroscopy."

optical identification of extragalactic radio sources. Quoting the latter paper (Morgan & Lesh 1965, page 1364), "Of the 'strong' sources identified, approximately one-half are associated with galaxies having the following characteristics: (a) they are located in clusters, of which they are outstandingly the brightest and largest members; (b) they are centrally located in their clusters; (c) they are never highly flattened in shape; and (d) they are of a characteristic appearance, having bright, elliptical-like [centers], surrounded by an extended amorphous envelope. These supergiant galaxies have been given the form-type class of cD in Morgan's [1958] classification."

This paper presents two new observational results:

1. Section 2 demonstrates that the velocity dispersion of the stars in the nearest, prototypical cD galaxy—NGC 6166 in the cluster Abell 2199—rises from values typical of giant elliptical galaxies near the center to the cluster dispersion in the cD halo. The halo also shifts toward the velocity of the cluster, which is different from that of NGC 6166. Thus the halo shares the dynamics of

individual galaxies in the cluster. We interpret this as evidence that the stars in the cD halo of NGC 6166 were stripped from the galaxies by fast collisions.

2. We measure the brightness profile of NGC 6166 to make quantitative Morgan's point (d) that cDs consist of a central elliptical plus a distinct, shallow-brightness-gradient halo. Photometry by Oemler (1976) suggested that NGC 6166 has such two-component structure. Our ideas about cD halos are based in large part on this result. However, we find that NGC 6166 is described by a single Sérsic (1968) profile at all radii outside the core. The cluster-dominated halo that is obvious in the kinematics is not obvious in the photometry. We need to rethink our understanding of how we recognize cDs and of whether cD galaxies are fundamentally different from other giant, core-boxy-nonrotating elliptical galaxies.

## 2. HOBBY–EBERLY TELESCOPE (HET) SPECTROSCOPY: VELOCITY AND VELOCITY DISPERSION PROFILES OF NGC 6166

### 2.1. History and Motivation

To distinguish between competing theories about the origin of cD galaxies (Section 8), a particularly powerful diagnostic is their internal kinematics. Does the velocity dispersion profile $\sigma(r)$ increase to the cluster velocity dispersion as one looks farther out into the part of the halo that encompasses many non-central cluster members? Is the systemic velocity of the halo similar to that of the central galaxy or is it similar to that of the cluster as a whole? Are these velocities ever different? This subject has a long history, and partial answers to these questions have been known for several decades.

#### 2.1.1. Systemic Velocities

Zabludoff et al. (1990) find that NGC 6166 has $(V_{cD} - \bar{V}) = 378 \pm 99$ km s$^{-1}$ for galaxy and cluster velocities of $V_{cD} = 9348 \pm 15$ km s$^{-1}$ and $\bar{V} = 8970 \pm 98$ km s$^{-1}$ (71 galaxies). Zabludoff et al. (1993) find that $V_{cD} = 9293 \pm 20$ km s$^{-1}$; $\bar{V} = 9063 \pm 104$ km s$^{-1}$; $(V_{cD} - \bar{V}) = 230 \pm 106$ km s$^{-1}$ for 68 cluster galaxies. Oegerle & Hill (2001) get peculiar velocities of $258 \pm 69$ to $346 \pm 73$ km s$^{-1}$, depending on how $\bar{V}$ is calculated and on how far out in the cluster the ($\sim$132) galaxies are counted. The derived peculiar velocity gets smaller as more galaxies get averaged. Among recent determinations, Coziol et al. (2009) get $V_{cD} = 9304$ km s$^{-1}$; $\bar{V} = 9143$ km s$^{-1}$; $(V_{cD} - \bar{V}) = 156$ km s$^{-1}$ for 471 cluster galaxies. The most up-to-date study by Lauer et al. (2014) gets $V_{cD} = 9317 \pm 10$ km s$^{-1}$; $\bar{V} = 9088 \pm 38$ km s$^{-1}$; $(V_{cD} - \bar{V}) = 229 \pm 39$ km s$^{-1}$ for 454 cluster galaxies.

Many cDs are essentially at rest at their cluster centers (e.g., Quintana & Lawrie 1982; Zabludoff et al. 1990; Oegerle & Hill 2001). Generally, cDs are more nearly at rest in their clusters than are non-cD first-ranked galaxies (e.g., Oegerle & Hill 2001; Coziol et al. 2009). But a significant fraction move at several hundred km s$^{-1}$ with respect to their clusters, often in association with cluster substructure, which suggests that a merger of two clusters is in progress (e.g., Oegerle & Hill 2001; Pimbblet et al. 2006; see also Beers & Geller 1983; Zabludoff et al. 1990, 1993). Proof of concept is provided by the Coma cluster. It is in the process of a cluster merger (White et al. 1993; Briel et al. 2001; Neumann et al. 2001, 2003;

Gerhard et al. 2007; Andrade-Santos et al. 2013; Simionescu et al. 2013). The NGC 4839 group is falling into the main Coma cluster, which itself has two central galaxies, NGC 4874 and NGC 4889, with different velocities (by about 680 km s$^{-1}$) and their own X-ray halos. NGC 4889 has a velocity of approximately $+430$ km s$^{-1}$ with respect to the Coma cluster. Only NGC 4874 is within $\lesssim 250$ km s$^{-1}$ of the cluster velocity. NGC 4874 and NGC 4889 are weak cDs, and NGC 4839 also shows signs of cD structure.

NGC 6166's velocity with respect to Abell 2199 is typical. *The diagnostic question is: does the halo of NGC 6166 have the same systemic velocity as its central galaxy or as its cluster? We find that the cD halo shows velocities between that of the galaxy and that of the cluster, approaching the cluster velocity at large radii. The observation that NGC 6166 is not centered in velocity in its cD halo is evidence that that halo does not belong dynamically or in its origin to the galaxy.*

#### 2.1.2. Velocity Dispersion Profiles

In a paper that fundamentally shaped our concept of cD galaxies, Dressler (1979) pushed measurements of velocity dispersions to then-unprecedented low surface brightnesses and showed that $\sigma(r)$ for IC 1101, the brightest galaxy in Abell 2029, rises with increasing radius $r$ from $\sim$375 km s$^{-1}$ at the center to $\gtrsim$500 km s$^{-1}$ at $r \simeq 71$ kpc. (The distance has been converted to the *WMAP* five-year cosmology distance scale, Komatsu et al. 2009; NED.) Thus the dispersion rises toward but does not reach the cluster $\sigma$ of 1160 km s$^{-1}$ (Coziol et al. 2009) or $1222 \pm 75$ km s$^{-1}$ (Lauer et al. 2014). Dressler interpreted this in the context of suggestions (Gallagher & Ostriker 1972; Ostriker & Tremaine 1975; Richstone 1976; White 1976; Merritt 1983; Richstone & Malumuth 1983) that cD halos consist of accumulated debris of stars stripped from cluster members by tidal encounters and by dynamical friction against the growing halo. Thus a cD consists of "a luminous but normal elliptical galaxy sitting in a sea of material stripped from cluster galaxies" (Richstone 1976; Dressler 1979). Dressler concludes (Dressler 1979, page 665): "The results of this study confirm an *[outward] increase in velocity dispersion, which is a necessary (but not sufficient) condition in the proof of the stripped debris hypotheses*." Sembach & Tonry (1996) and Fisher et al. (1995) confirm these results.

Not surprisingly, the most thoroughly studied cD is the nearest one. M87 is marginally a cD in that it has extra light at large radii with respect to an $n \simeq 9^{+2}_{-1}$ Sérsic fit (Figure 50 in Kormendy et al. 2009; hereafter KFCB). This is a normal Sérsic index for a core-boxy-nonrotating elliptical, but the amount of extra light is small, and in fact, an $n = 11.8^{+1.8}_{-1.2}$ Sérsic function fits the whole profile outside the core. This Sérsic index is outside the range normally observed for core-boxy-nonrotating Es. Nevertheless, a cD halo cannot securely be identified as an outer component that is photometrically distinct from the main body of the galaxy. At the same time, it is clear that the Virgo cluster does contain intracluster stars, from broad-band surface photometry (Mihos et al. 2005, 2009; Mihos 2011), from spectroscopy of individual stars (Williams et al. 2007b), and from the detection of intracluster globular clusters (Williams et al. 2007a) and planetary nebulae (Arnaboldi et al. 1996, 2002, 2004; Castro-Rodriguéz et al. 2009; Arnaboldi & Gerhard 2010; Arnaboldi 2011). The intracluster light (ICL) is irregular in spatial distribution and defined largely by (tidal?) streams. We conclude that it is in

early stages of formation. The streams support our conclusion that the ICL consists of stars that were stripped from individual galaxies. Kormendy & Bender (2012) present additional evidence that disk galaxies in Virgo have very substantially been dynamically heated. The ICL pervades the cluster and must feel the cluster gravitational potential. And the outer halo of M87 merges seamlessly with this ICL (Mihos papers). Do we observe that the velocity dispersion of stars in M87 increases toward the cluster dispersion?

The answer—tentatively—is yes. The integrated light shows an outward drop in $\sigma$ from ~360 km s$^{-1}$ in the central few arcsec to ~300 km s$^{-1}$ at $20'' \lesssim r \lesssim 100''$ and then an outward rise to ~340 km s$^{-1}$ at $r \sim 250''$ (Murphy et al. 2011, 2014). This is subtle and not easily interpreted. But the upward trend in $\sigma$ continues in the globular cluster population, which reaches $\sigma \simeq 400$–470 km s$^{-1}$ by $r \sim 380''$ (Wu & Tremaine 2006; see Côté et al. 2001 for earlier results). Planetary nebula data in Doherty et al. (2009) reveal both M87 halo and intracluster stars, but the data are too sparse to determine a $\sigma(r)$ profile. Also, though they do not overlap greatly in radial leverage, stellar dynamical models and mass profile measurements from the X-ray gas give essentially consistent results (e.g., Churazov et al. 2008; Gebhardt & Thomas 2009). Thus, M87 is the nearest galaxy where various test particles have been used to probe the dynamics of a marginal cD from its center out to radii where the cluster dominates. The problem is that the test particles are hetero-geneous enough and the statistics for point particles are poor enough so that we cannot securely see the transition from the galaxy's main body to any halo that is controlled by cluster gravity. Nevertheless, as a proof of concept, M87 is important. And it provides a hint that proves to be prescient: the dispersion profile starts to rise at $r \sim 100'' \sim 8$ kpc, well interior to the radii where any plausible argument identifies the beginning of a cD halo based on photometry alone.

Outward $\sigma$ rises in cD or cD-like galaxies are reported by Carter et al. (1981, 1985) and by Ventimiglia et al. (2010). Still, the only prototypical cD in which the velocity dispersion of the stellar halo is robustly seen to rise toward larger radii by several authors is NGC 6166 in the cluster Abell 2199. From a central velocity dispersion of $\sigma \sim 300$ km s$^{-1}$, the dispersion first drops outward and then rises to $\sigma \sim 400$ km s$^{-1}$ (Carter et al. 1999) at about $30''$. The outermost dispersion measure-ments by Kelson et al. (2002) are $\sigma = 529 \pm 74$ km s$^{-1}$ at $r = 39''$ and $\sigma = 663 \pm 121$ km s$^{-1}$ at $r = 58''$. Abell 2199's cluster dispersion is $\sigma = 819 \pm 32$ km s$^{-1}$ (Lauer et al. 2014). *No velocity dispersion measurments of any cD galaxy reach large enough radii to show that $\sigma$ increases all the way up to the cluster dispersion.*

*The first purpose of this paper is to push the measurements of NGC 6166 far enough out in radius to see whether or not $\sigma(r)$ reaches the cluster dispersion.*

### 2.2. HET Spectroscopy

We obtained spectra at three slit positions (Figure 1) along and near the major axis of NGC 6166 with the 9.2 m HET and Low Resolution Spectrograph (LRS: Hill et al. 1998). The slit width was $1\overset{''}{.}5$, the reciprocal dispersion was 116 km s$^{-1}$ pixel$^{-1}$, and the resolution expressed as a velocity dispersion was $\sigma_{\mathrm{instr}} = 125$ km s$^{-1}$. The slit positions had exposure times of $8 \times 900$ s ("center," with NGC 6166 centered well inside the slit), $4 \times 900$ s ("offset" position along the major axis, centered on the bright, elongated galaxy NGC 6166A visible in

Figure 1), and $6 \times 900$ s $+ 1 \times 800$ s ("alternate" position offset by $11\overset{\circ}{.}5$ from the major axis but on the other side of the center, positioned to miss star and galaxy images). All individual exposures were taken on different nights. The standard star spectrum used is a combination of HD 74377 and HR 2600 which reproduces line strengths of massive elliptical galaxy spectra well and minimizes template mismatch. In any case, the kinematics were measured with Bender's (1990) Fourier correlation quotient method, which is designed to eliminate template bias. Errors were calibrated with Monte Carlo simulations.

Figure 2 shows an unsharp-masked version of the sum of the best spectra along the central slit position (*white line* in Figure 1). By dividing out the brightness profile of the galaxy, we can see absorption lines and qualitatively judge S/N from the center out to the largest radii. The strongest lines in NGC 6166, Mg b, Na D, and H$\beta$, are visible all the way to the companion galaxy on the slit. Even Fe $\lambda$ 5270 Å and 5335 Å are visible quite far out (see also Figure 3). They are used in Section 6 to measure [$\alpha$/Fe] overabundance out into the part of the halo where the velocity dispersion is large. Most important, Figure 2 already shows that all lines except Na D get very wide in the cD halo of NGC 6166.

The Na D line is narrow at all radii and shows little gradient in velocity. It gives a dispersion of $\sigma_{\mathrm{Na\,D}} \simeq 300$ km s$^{-1}$ at all radii. We assume that the line is produced by interstellar gas and do not include it in the wavelength region from redward of the iron lines to blueward of H$\beta$ that we use for $V$ and $\sigma$ measurements. Dust is seen near the center in Figure 8. There may be a more smoothly distributed ISM at larger radii, as suggested also by the fact that H$\beta$ absorption in our spectra is significantly weaker than even a very old stellar population would show. However, it is not obvious that its kinematics should be a simple as we measure with the Na D line. Interpretation of this line in the context of the X-ray gas halo of the galaxy is beyond the scope of this paper.

The offset and alternate slit positions yielded poorer spectra. We discard one spectrum taken with too much moonlight, so the alternate slit position has only six good spectra. Of these, one is fainter than normal by ~14% and two more are fainter by ~23%, presumably due to clouds. (The observations are queue-scheduled, so we cannot personally monitor the observing conditions. However, we checked that the galaxy was centered on the slit. Seeing is relatively unimportant.)

Offset sky spectra were taken after all NGC 6166 exposures. For the center slit position, these were cleaned of bad pixels and averaged to give high S/N and then used for all sky subtractions. Each spectrum was individually sky-subtracted before the spectra were added. The sky subtraction of the central slit spectra is good (Figure 2). However, for the other two slit positions, most sky spectra could not be used for sky subtraction because too many night sky emission lines changed in strength in the short time between exposures. For the offset sky positions, the sky was measured as far from the galaxy as possible; since even the NGC 6166 end of the slit is far from the galaxy (Figure 1), these sky spectra should be essentially free of galaxy light. However, for the alternate slit position, sky spectra taken from the galaxy images do subtract a little halo light. For this reason—as well as problems with moonlight and with clouds—the alternate slit position does not reach as far out as the primary slit position illustrated in Figure 2. In addition,
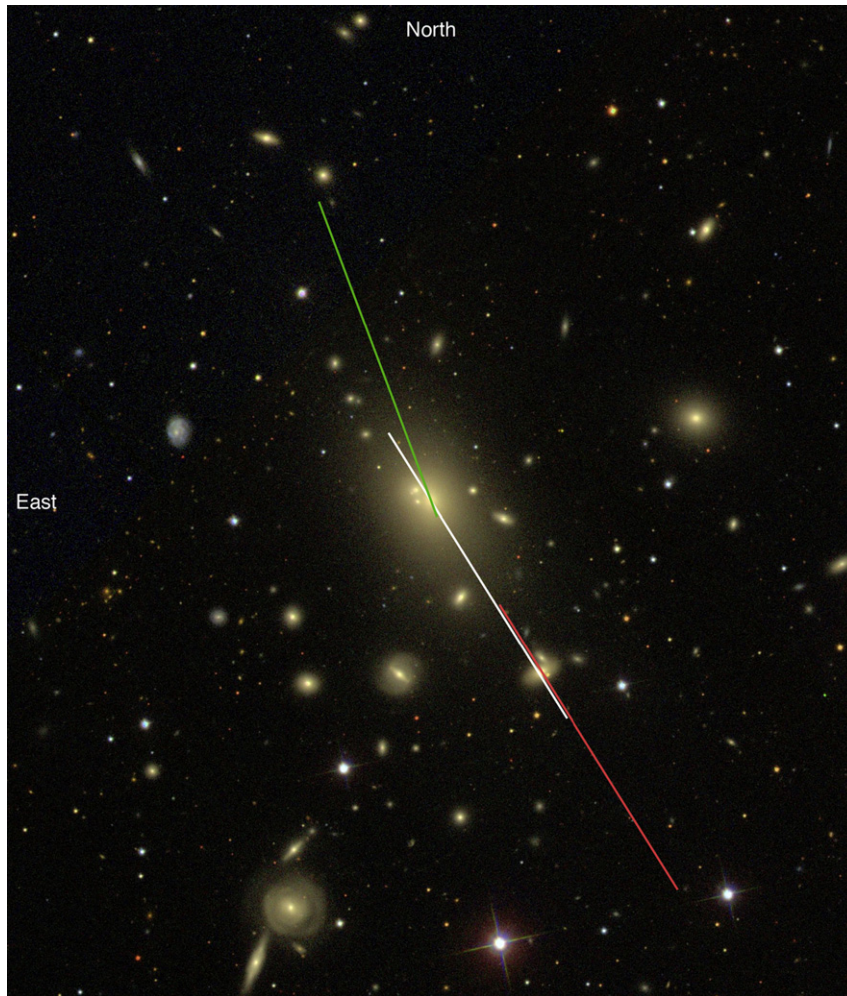
**Figure 1.** SDSS *gri*-band color image of Abell 2199 showing our three slit positions superposed on NGC 6166. This figure illustrates the slit length in the trimmed spectra, 480, $0\rlap{.}''47$ pixels $= 225\rlap{.}''6 = 3\rlap{.}'76$. The image is from `http://www.wikisky.org`. In the text, the slit positions are referred to as (*white*) central, (*red*) offset, and (*green*) alternate. Results from these slits are listed in Table 1 and plotted in Figures 4, 5, and 15–18 in black, red, and green, respectively.

we found that we got the best results to the largest radii in the alternate slit position by using only the four best spectra.

Figure 3 shows sample spectra for five radial bins in NGC 6166 and for the optimized template star. This binning is used in Section 6 to measure line strengths for the Mg b and Fe lines. Reliable line strength measurements are possible out to the bin at $r = 59''$. Velocity dispersions are easier—they are measureable for the $r = 87''$ bin and for several others at large radii in the center, alternate, and offset slit positions.

### 2.3. Kinematic Results

The summed center, alternate, and offset spectra were reduced with the Fourier correlation quotient program of Bender (1990). This gives velocity $V$, velocity dispersion $\sigma$, the higher-order Gauss–Hermite coefficients $h_3$ and $h_4$, and nonparametric line-of-sight velocity distributions (LOSVDs). At some radii near $r \sim -12''$ (see Figure 2), the LOSVDs show a main peak at the systemic velocity of NGC 6166 and smaller peak in its wings associated with another of the multiple nuclei. We omitted the corresponding velocity bins from the LOSVD fit. Since neither the center nor the radii where $\sigma$ starts to climb are affected, this cleaning does not affect our conclusions.

However, many published $V$ and $\sigma$ measurements show contamination from the multiple nuclei.

The instrumental velocity dispersion was measured in our reduced spectra to be $\sigma_{\mathrm{instr}} = 125\,\mathrm{km\,s}^{-1}$, easily adequate for the galaxy dispersions $\sigma \gtrsim 300\,\mathrm{km\,s}^{-1}$ studied in this paper.

The kinematics are listed in Table 1 and shown in Figure 4.

### 2.4. The Velocity Profile of NGC 6166

The systemic velocity of NGC 6166 is $206 \pm 39\,\mathrm{km\,s}^{-1}$ higher than the velocity $9088 \pm 38\,\mathrm{km\,s}^{-1}$ of 494 cluster galaxies (Lauer et al. 2014). Here we use our measure of the systemic velocity of NGC 6166, $V_{\mathrm{cD}} = 9294 \pm 10\,\mathrm{km\,s}^{-1}$. It is consistent within errors with values in Zabludoff et al. (1993) and in Coziol et al. (2009). Other, inconsistent published measurements may be affected by contamination by the multiple nuclei. Using our $V_{\mathrm{cD}}$, NGC 6166 moves at $(0.25 \pm 0.05)\sigma$, typical of the values found by Lauer et al. (2014).

If the cD halo consists of tidal debris, then we expect that its systemic velocity should shift toward that of the cluster at the radii where $\sigma$ rises toward the cluster value. Figure 4 shows that the velocity at large radii does decrease from $V_{\mathrm{cD}}$ toward the cluster velocity. The average of the large-radius points is only
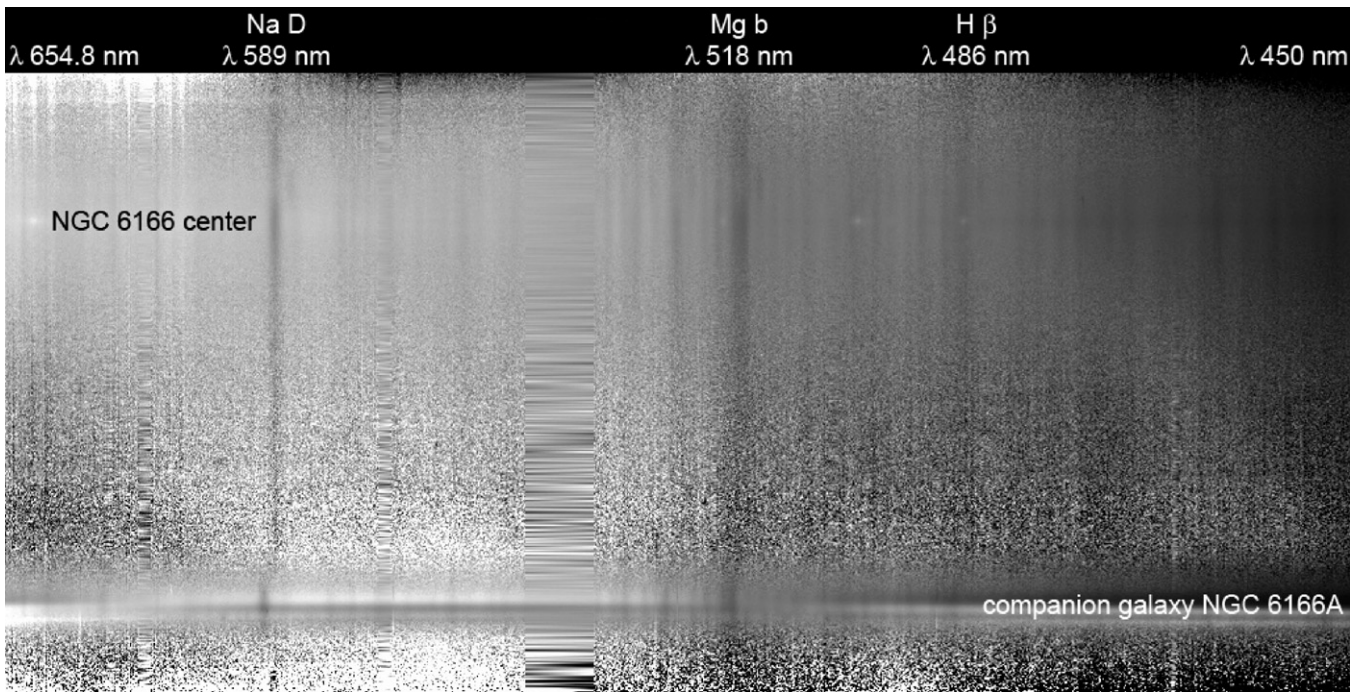
**Figure 2.** Unsharp-masked central spectrum of NGC 6166 (*white line* in Figure 1). This is the sum of eight, 900 s exposures divided by an image each of whose columns is the mean of a central block of columns near the Mg b lines in the original spectrum. This divides out the brightness profile of the galaxy and shows the spectral lines at all radii (*vertical*) and wavelengths (*horizontal*; the wavelenth range is labeled at the top). Several absorption lines are labeled. We have interpolated through three badly subtracted night sky lines. The center of NGC 6166 and of the companion galaxy NGC 6166A that is on the slit (Figure 1) are also labeled. Note also that one of the multiple nuclei—the one nearest the slit on the side of NGC 6166 opposite to NGC 6166A in Figure 1—contributes visible NaD and Mg b absorption lines at small radii above the center of NGC 6166 and blueward of the galaxy line. Their contributions to the line-of-sight velocity distributions were omitted from our fits. We also see faint central emission lines of H$\beta$, [O III] $\lambda$ 5007 Å, and [N I] $\lambda$ 5199 Å. In kinematic measurements, we iteratively corrected for these lines by replacing them with the broadened star spectrum over the few pixels in which they affect the measurements. The important result shown by this figure is that the Mg b lines get very broad at large radii from NGC 6166, whereas the Na D lines do not.

$\sim -70\,\mathrm{km\,s^{-1}}$. Still, the inner cD halo of NGC 6166 is more nearly at rest within the cluster than is the central galaxy.

The measurement of the velocity difference between the cD halo and the cluster is more difficult that the measurement that the halo $\sigma$ is a factor of $\sim$3 larger than the central $\sigma$ of NGC 6166. NGC 6166's peculiar velocity is only 25% of the cluster $\sigma$, twice as big as the error bars in the *V* measurements. (The *V* and $\sigma$ errors are comparable; see Table 1.) Moreover, some halo stars that are nearest to NGC 6166 may be pulled slightly toward the galaxy velocity. So the *V* comparison is more difficult and less obviously successful than the $\sigma$ comparison. But we do see a shift in halo *V* toward the cluster velocity on both sides of the center. This supports our picture that the halo stars were stripped from many cluster galaxies.

### 2.5. The Velocity Dispersion Profile of NGC 6166

Figure 5 compares our kinematic results on NGC 6166 with published dispersion profiles. Carter et al. (1999) and Kelson et al. (2002) observed much of the rise in $\sigma$ to the cluster value. However, our observations are the first to reach deep enough to see $\sigma$ for the intergrated starlight in a cD halo rise all the way to the cluster dispersion in any galaxy cluster.

The Carter et al. (1999) data are not shown in Figure 5, because they did not publish a table of their results. Their outermost measurements at radii of 30″–36″ are $\sigma \simeq 390, 361$, and 438 km s$^{-1}$. These are consistent with our results and with Kelson's. (However, Carter et al. 1999 derive velocities that increase as *r* increases; they interpret this as "modest major-axis rotation." Kelson et al. 2002 also see "systematic rotation $[V/\sigma \approx 0.3]$ in the intracluster stars beyond 20 kpc." We do not

see rotation; rather, the halo velocity decreases toward the cluster velocity on both sides of the center.)

Tonry (1984, 1985) measured the multiple nuclei of NGC 6166 but did not reach far enough out to see an outward increase in $\sigma$. Similarly, Fisher et al. (1995) and Loubser et al. (2008) measured only a slight outward drop in $\sigma$ in the main body of the galaxy.

Figure 5 illustrates the most important result in this paper: *The velocity dispersion in NGC 6166 increases outward to a weighted mean of $\sigma = 865 \pm 58\,km\,s^{-1}$ for the four data points at $r = 83''$–$107''$. This equals the velocity dispersion $\sigma = 819 \pm 32\,km\,s^{-1}$ for 454 galaxies in Abell 2199 (Lauer et al. 2014). The rise in $\sigma$ to the cluster velocity dispersion is consistently implied by all three of our slit positions. This result is the strongest evidence that the cD halo of NGC 6166 is made of stars that have been accreted in minor mergers or stripped from cluster galaxies by dynamical harassment.*

## 3. SURFACE PHOTOMETRY: DOES NGC 6166 HAVE A PHOTOMETRICALLY DISTINCT HALO?

### 3.1. The Standard Picture of cD Halos

Our standard picture of the nature of cD halos and the way in which we identify cD galaxies are based in large part on photometry of NGC 6166 and other cD galaxies by Oemler (1976). Oemler's procedures and conclusions were later made quantitative by Schombert, as discussed below. But the iconic, two-component structure suggested by Oemler's photometry of cDs—particularly NGC 6166—firmly cemented in our minds the notion that cDs consist of an elliptical-galaxy-like central
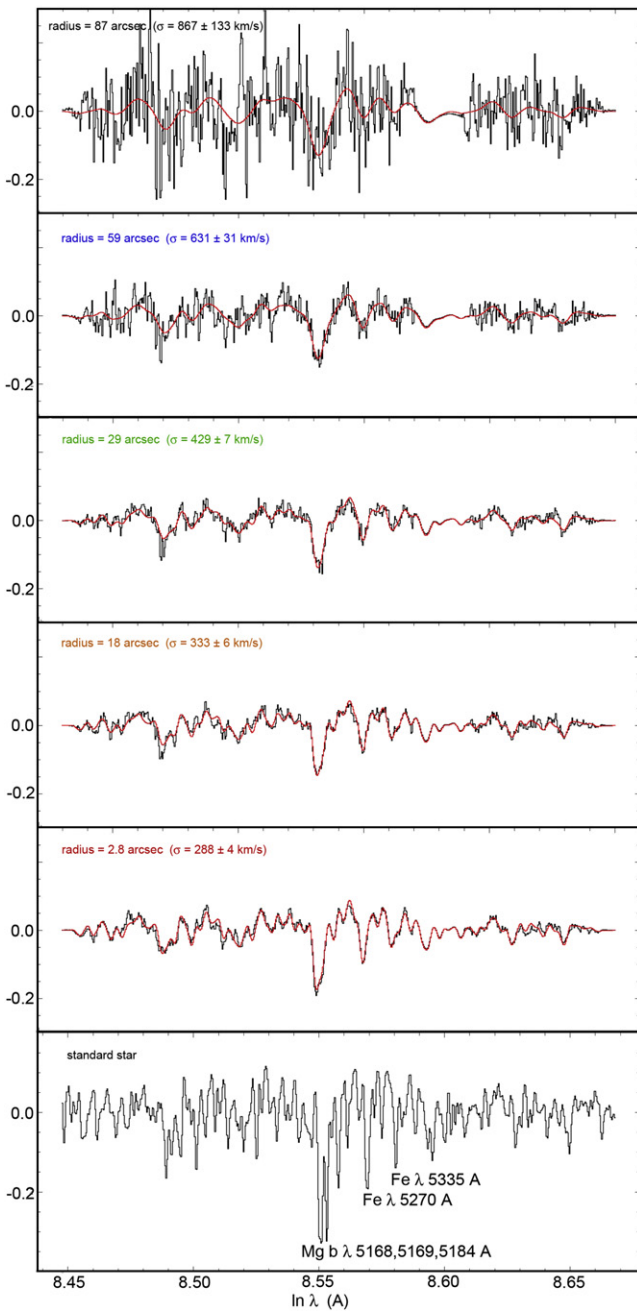
**Figure 3.** Spectra of NGC 6166 at various radii along the center slit position (*black*) fitted (*red*) with the spectrum of the template star (*bottom panel*) broadened to the line-of-sight velocity distribution given by the Fourier correlation quotient program. To improve the S/N for this illustration, more rows are averaged here into each radial bin than are averaged for the kinematic reductions in the next section. This coarser binning is also needed for line-strength measurements. Therefore, the radial bins used here and the color scheme used in the keys is the same as it is in Section 6 and Figure 21 on heavy element abundances.

body plus a *photometrically distinct*, shallower-surface-brightness halo that is not present in normal giant ellipticals. Oemler's profile of NGC 6166—augmented by *Hubble Space Telescope* (*HST*) photometry to improve the central spatial resolution—is shown in Figure 6.

The clearly two-humped profile in Figure 6 decisively quantifies Morgan's description of his visual impression of two-component structure. Other cDs in Oemler (1976), in Schombert (1986, 1987, 1988), and in other papers from the

same era behave similarly. The picture of cD halos that has been in our minds ever since is made still more concrete using modern profile analysis machinery by decomposing the profile into two Sérsic (1968) functions. Several recent papers have done this and suggested that the inner components are normal ellipticals whereas the cD halos have exponential profiles (Seigar et al. 2007; Donzelli et al. 2011). In fact, the Sérsic–Sérsic decomposition in Figure 6 requires that the cD halo have $n \simeq 0.77$, between an exponential ($n = 1$) and a Gaussian ($n = 0.5$) in its outer cutoff. A worrying hint is that the inner profile has $n = 1.62$, smaller than we have found for any other elliptical (KFCB). Note that, in making this fit, we have been very conservative about excluding the inner, shallow-power-law core (see Kormendy et al. 1994; Lauer et al. 1995, and KFCB for the definition of cores and Gebhardt et al. 1996; Kormendy 1999, and Lauer et al. 1995 for a demonstration that they are features of the unprojected and not just the projected profiles). We also omit the central active galactic nucleus (AGN) from the fit. About 2/3 of the light of the profile in Figure 6 is in the cD halo.

The ideas summarized above were made more quantitative by Schombert (1988). Schombert (1986, 1987) measured average surface brightness profiles of non-first-ranked ellipticals as functions of galaxy absolute magnitude $M_V$ in seven $M_V$ bins from −17 to −22.5 (he used $H_0 = 50 \text{ km s}^{-1} \text{ Mpc}^{-1}$). Schombert (1988) then used these template profiles to define cD galaxies. First, the template profile is found that best matches the inner profile of the candidate galaxy over the largest possible radius range. If this profile fits all of the candidate galaxy to within the scatter seen among the individual profiles that were used to make the template, then this galaxy is an ordinary elliptical. In contrast (Figure 1 in Schombert 1988; cf. Figure 6 here), if the galaxy in question has a giant outer halo above the template profile fitted to the inner parts, then the galaxy is a cD and the integrated difference between its observed profile and the best-fitting template is the cD halo. This definition is similar in spirit to one used by Oemler (1976) but has the advantage of allowing the profiles of ellipticals to depend on luminosity. And it has the virtue of being nonparametric—it does not depend on describing the inner profile with an analytic fitting function.

The profile decomposition shown in Figure 6 is nothing more nor less than Schombert's procedure in parametric form, using Sérsic functions for the inner and outer components. Much experience in recent years has shown that Sérsic functions are excellent fits to elliptical-galaxy profiles (see KFCB for data and review) and hence also to Schombert's template profiles. However:

*We find a problem with our canonical picture of cD halos (Section 3.2). The photometry shown in Figure 6 is in error. Our composite profile measurements of NGC 6166 are very well fitted by a single Sérsic function at all radii outside the central core. In contrast to our kinematic results, there is no photometric hint of two-component structure.*

### 3.2. Composite V-band Brightness Profile of NGC 6166

We have measured the *V*- and *I*-band surface brightness profiles of NGC 6166 using CCD images from four ground-based telescopes and four cameras (WFPC1 PC, WFPC2 WF, ACS, and NICMOS2) on *HST*. Parameters of the images are listed in Table 2. This section discusses the *V*-band profile.

<div align="center">

**Table 1**
Fourier Correlation Quotient Kinematic Measurements of NGC 6166

</div>

| Radius (arcsec) | $V$ (km s$^{-1}$) | $\epsilon\,(V)$ (km s$^{-1}$) | $\sigma$ (km s$^{-1}$) | $\epsilon\,(\sigma)$ (km s$^{-1}$) | $h_3$ | $\epsilon\,(h_3)$ | $h_4$ | $\epsilon\,(h_4)$ | S/N (Å$^{-1}$) |
|---|---|---|---|---|---|---|---|---|---|
| −29.55 | −36 | 17 | 416 | 30 | −0.080 | 0.037 | 0.219 | 0.037 | 32 |
| −2.79 | −2 | 3 | 294 | 5 | 0.010 | 0.011 | 0.054 | 0.011 | 110 |
| −0.97 | 4 | 3 | 298 | 4 | 0.012 | 0.010 | 0.022 | 0.010 | 112 |
| 0.43 | 1 | 4 | 301 | 5 | 0.037 | 0.011 | 0.031 | 0.011 | 109 |
| 2.04 | −3 | 3 | 311 | 5 | 0.007 | 0.010 | 0.050 | 0.010 | 116 |
| 5.09 | 4 | 3 | 302 | 5 | 0.012 | 0.011 | 0.053 | 0.011 | 111 |
| 9.87 | −2 | 5 | 330 | 7 | 0.008 | 0.013 | 0.081 | 0.013 | 89 |
| 16.57 | −17 | 6 | 362 | 9 | −0.012 | 0.016 | 0.106 | 0.016 | 75 |
| 26.15 | −38 | 13 | 448 | 20 | 0.037 | 0.026 | 0.129 | 0.026 | 45 |
| 37.65 | −44 | 18 | 495 | 29 | −0.003 | 0.033 | 0.144 | 0.033 | 36 |
| 51.88 | −17 | 36 | 574 | 46 | 0.000 | 0.057 | 0.036 | 0.057 | 21 |
| 66.07 | −90 | 70 | 732 | 96 | 0.003 | 0.086 | 0.069 | 0.086 | 14 |
| 82.62 | −49 | 87 | 853 | 76 | 0.064 | 0.093 | −0.105 | 0.093 | 13 |
| 106.8 | 29 | 118 | 886 | 111 | 0.297 | 0.121 | −0.083 | 0.121 | 10 |
| −87.85 | −56 | 285 | 986 | 336 | ... | ... | ... | ... | 7 |
| −64.12 | −63 | 86 | 606 | 102 | ... | ... | ... | ... | 13 |
| −47.67 | −31 | 45 | 474 | 53 | ... | ... | ... | ... | 20 |
| −33.57 | −50 | 23 | 419 | 28 | ... | ... | ... | ... | 34 |
| −22.99 | −34 | 16 | 352 | 19 | ... | ... | ... | ... | 41 |
| −17.59 | −37 | 14 | 363 | 16 | ... | ... | ... | ... | 50 |
| −9.60 | −24 | 7 | 273 | 9 | ... | ... | ... | ... | 69 |
| −7.01 | −4 | 7 | 277 | 9 | ... | ... | ... | ... | 70 |
| −4.90 | −14 | 7 | 279 | 8 | ... | ... | ... | ... | 80 |
| −3.02 | −5 | 5 | 284 | 6 | ... | ... | ... | ... | 98 |
| −1.61 | −1 | 7 | 297 | 8 | ... | ... | ... | ... | 84 |
| −0.67 | 4 | 7 | 310 | 8 | ... | ... | ... | ... | 89 |
| 0.04 | −1 | 7 | 307 | 8 | ... | ... | ... | ... | 85 |
| 0.51 | −3 | 7 | 310 | 8 | ... | ... | ... | ... | 83 |
| 0.98 | 6 | 8 | 299 | 9 | ... | ... | ... | ... | 74 |
| 1.68 | 7 | 6 | 306 | 7 | ... | ... | ... | ... | 98 |
| 3.09 | 12 | 5 | 295 | 6 | ... | ... | ... | ... | 111 |
| 4.97 | 12 | 7 | 286 | 9 | ... | ... | ... | ... | 72 |
| 7.32 | 15 | 6 | 282 | 8 | ... | ... | ... | ... | 83 |
| 105.0 | −125 | 153 | 841 | 180 | ... | ... | ... | ... | 11 |

**Note.** The columns list radius with negative radius on the NE side of the center, velocity $V$ with respect to the systemic velocity and its estimated error $\epsilon\,(V)$, velocity dispersion $\sigma$ and its estimated error $\epsilon\,(\sigma)$, and the $h_3$ and $h_4$ Gauss–Hermite moments of the line-of-sight velocity distribution (LOSVD) and their respective errors $\epsilon\,(h_3)$ and $\epsilon\,(h_4)$, and the signal-to-noise ratio for the binned spectrum. When no values of $h_3$ and $h_4$ are given, then the LOSVDs were fitted with Gaussians. The first block of results are for the center slit position; the second block is for the alternate slit position; and the third block is for the offset slit position.

The central profile is from an *HST* WFPC1 measurement by Lauer et al. (1995), from our measurement of an *HST* WFPC2 F555W image (GO program 7265; D. Geisler, P. I.), and from our high-resolution (Gaussian dispersion radius $\sigma_* = 0\rlap{.}{''}32$) *V*-band image from the Canada–France–Hawaii Telescope (CFHT) Cassegrain camera. The CFHT observing run is discussed in KFCB. The three images give independent *V*-band zeropoints that agree (fortuitously) to much better than ±0.01 mag arcsec$^{-2}$. The three zeropoints have been averaged.

Similar in resolution to the CFHT Cassegrain image is a *g* image from the CFHT MegaCam. We also include photometry of an *r* image from SDSS; it is used over a larger radius range to derive the *I*-band profile in the next subsection, but it is used here to help to tie together small and large radii, and it helps to measure the ellipticity and PA profile. The outer profile is obtained using a *g*-band image from the Wendelstein Observatory's new 2 m Fraunhofer Telescope and a *V*-band image from the McDonald Observatory 0.8 m telescope. The latter profile

reaches $r = 416''$, where $\mu = 27.28$ *V* mag arcsec$^{-2}$. The *V*-band profile of NGC 6166 is similar in accuracy and limiting surface brightness to the data in KFCB.

Figure 7 shows the raw profiles. Three kinds of profiles are shown. Most are based on isophote fits as in Bender (1987), Bender & Möllenhoff (1987), and Bender et al. (1987, 1988). The algorithm fits ellipses to the galaxy isophotes; it calculates the ellipse parameters surface brightness, isophote center coordinates $X_{\rm cen}$ and $Y_{\rm cen}$, major and minor axis radii, ellipticity $\epsilon$, and position angle PA of the major axis. Radial deviations of the isophotes from the ellipses are expanded in a Fourier series in the eccentric anomaly $\theta_i$,

$$\Delta r_i = \sum_{k=3}^{N} \left[ a_k \cos\left(k\theta_i\right) + b_k \sin\left(k\theta_i\right) \right]. \qquad (1)$$

The most important parameter is $a_4$, expressed in the figures as a percent of the major-axis radius $a$. If $a_4 > 0$, the isophotes are
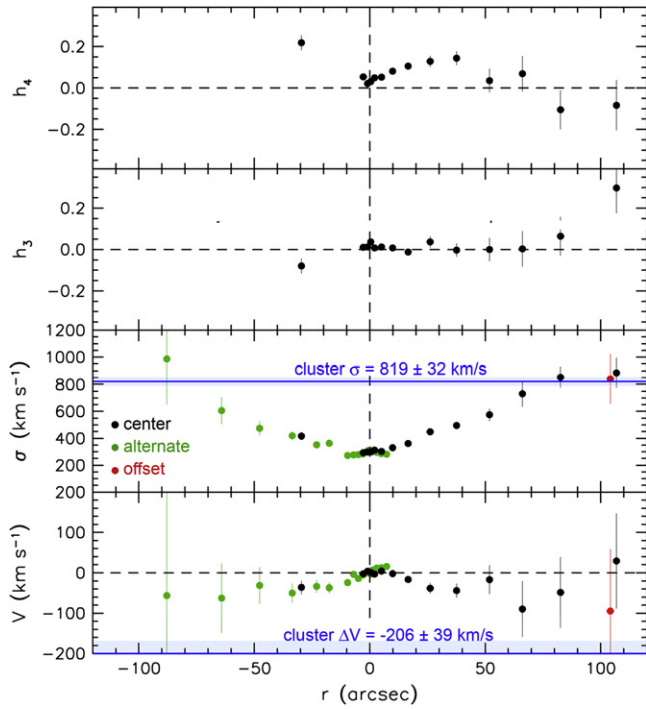
**Figure 4.** Stellar kinematics (nearly) along the major axis of NGC 6166 from the center, alternate, and offset slit spectra. Velocities and radii are not folded around the center; positive radii are in the direction of the cluster galaxy NGC 6166A in Figure 1; i.e., SW of NGC 6166. The panels show (*bottom–top*) velocity $V$ with respect to the systemic velocity of NGC 6166, velocity dispersion $\sigma$, and the Gauss–Hermite coefficients $h_3$ and $h_4$. The cluster systemic velocity with respect to NGC 6166 and its velocity dispersion are shown in blue (Lauer et al. 2014).
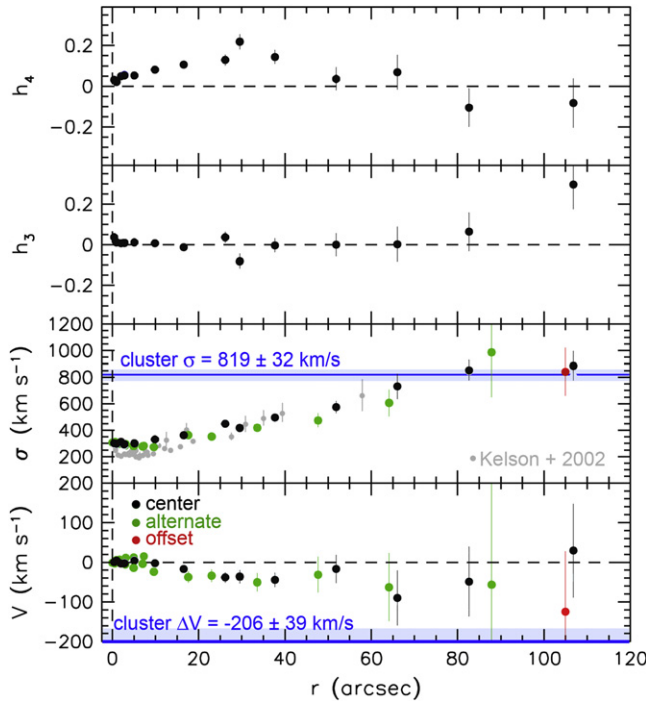


**Figure 5.** NGC 6166 kinematic measurements from Figure 4 folded in radius around the center and compared with the velocity dispersion profile obtained by Kelson et al. (2002). Note that, whereas $r$ has been replaced with $|r|$, the sign of $V$ has not been changed. Again, the cluster systemic velocity with respect to NGC 6166 and its velocity dispersion are shown in blue.
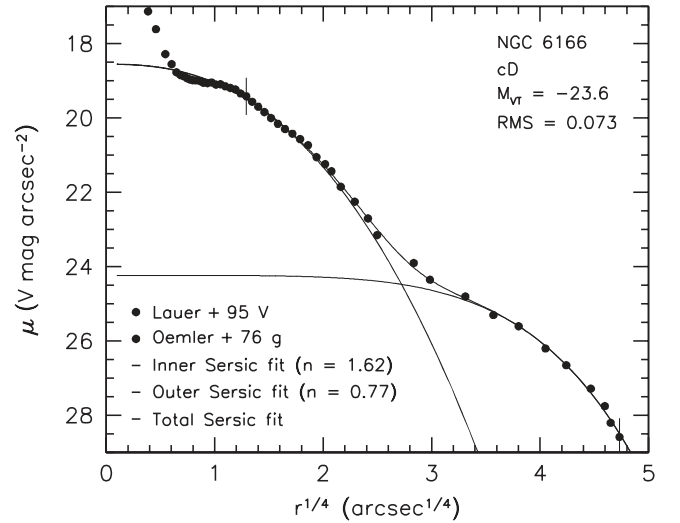


**Figure 6.** Circles show an average of the major-axis profile of NGC 6166 measured with *HST* by Lauer et al. (1995) and the outer profile measured by Oemler (1976). The lines show a photometric decomposition into two Sérsic functions in the radius range shown by the vertical dashes across the profile. The Sérsic indices and fit rms in mag arcsec$^{-2}$ are given in the key.

**Table 2**
Photometry Data Sources

| No. | Telescope and Instrument | Filter | Scale (arcsec pixel$^{-1}$) | Field of View (arcmin) |
|---|---|---|---|---|
| 1 | *HST* WFPC1 PC | F555W | 0.043 | 0.6 × 0.6 |
| 2 | *HST* WFPC2 WF | F555W | 0.10 | 2.7 × 2.7 |
| 3 | *HST* ACS | F475W, F814W | 0.050 | 3.5 × 3.4 |
| 4 | *HST* NICMOS2 | F160W | 0.076 | 0.4 × 0.4 |
| 5 | CFHT Cass | V | 0.22 | 7.0 × 7.0 |
| 6 | CFHT MegaCam | g | 0.187 | 57.6 × 56.4 |
| 7 | Wendelstein 2 m | g | 0.20 | 27.6 × 29.0 |
| 8 | SDSS | r | 0.396 | … |
| 9 | McDonald 0.8 m PFC | V | 1.36 | 46 × 46 |

**Note.** The *V*-band zeropoint is an average of zeropoints from WFPC1 F555W, WFPC2 F555W, and CFHT Cass. The three zeropoints agree to a few thousandths of a mag arcsec$^{-2}$. The *I*-band zeropoint is from ACS F814W. All magnitudes are VEGAMAG. The composite profiles $\mu(r)$ are constructed by shifting together the individual profiles from each telescope to minimize the scatter in $\mu$. The Wendelstein camera is described in Kosyra et al. (2014).

disky-distorted; large $a_4$ at intermediate radii would indicate an S0 disk. If $a_4 < 0$, the isophotes are boxy. The importance of these distortions is discussed in Bender (1987, 1988), Bender et al. (1987, 1988, 1989, 1994), Kormendy & Djorgovski (1989), Kormendy & Bender (1996), KFCB, Kormendy (2009), and below.

Some profiles were measured using Lauer's (1985) program `profile` in the image processing system VISTA (Stover 1988). The interpolation algorithm in `profile` is optimized for high spatial resolution, so it is best suited to our high-S/N images of the core of NGC 6166. The isophote calculation is Fourier-based, so it not well suited to measuring the outer parts of NGC 6166, where masking of other galaxies in the cluster results in very incomplete isophotes.
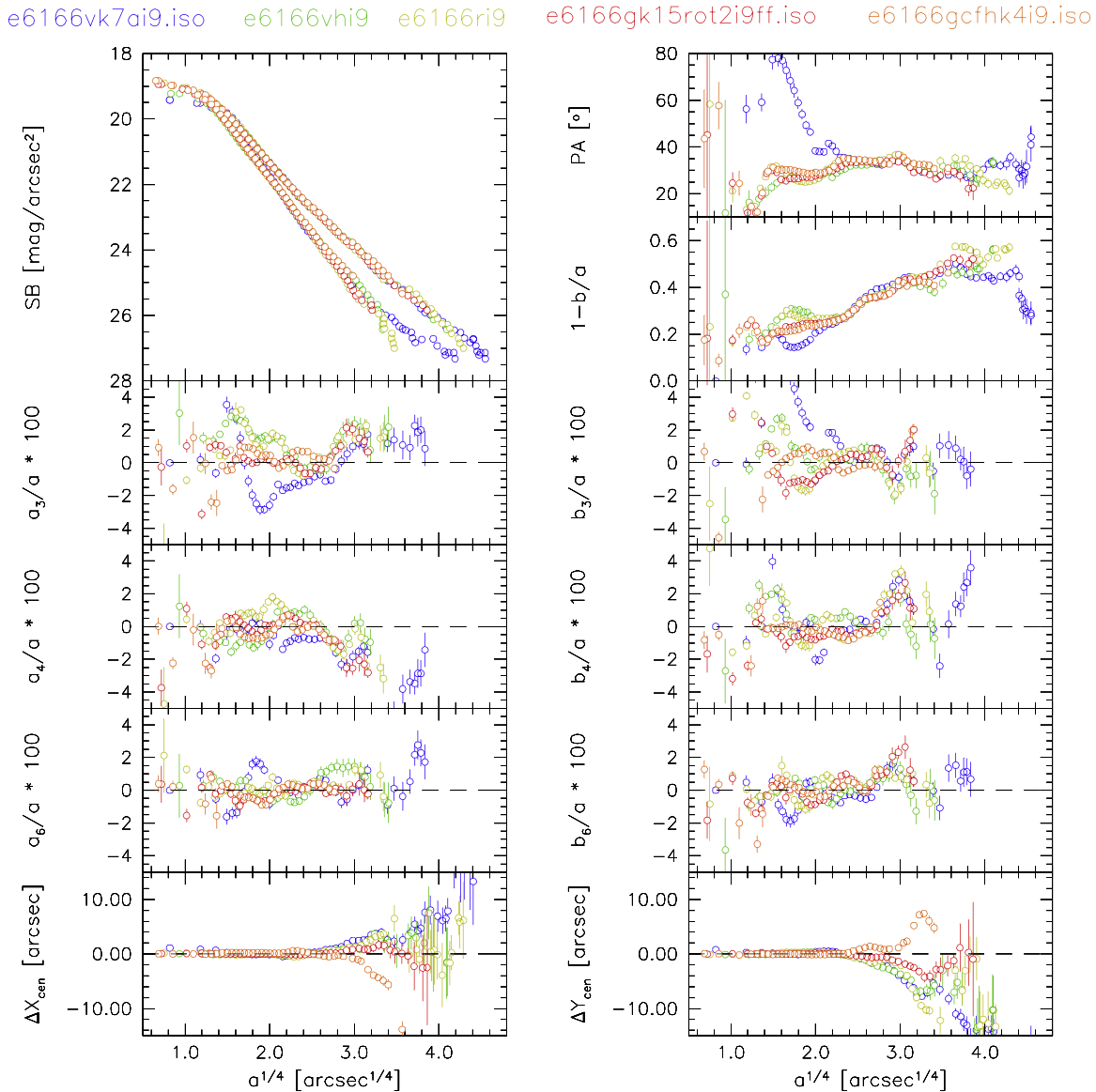
**Figure 7.** Points in various colors show our surface photometry of NGC 6166 images from four telescopes, all zeropointed to the *V*-band *HST* profile from Lauer et al. ([1995](#)). Here SB is surface brightness, *b/a* is isophote axial ratio, $1 - b/a$ is ellipticity, PA is position angle east of north, and $a_n$ and $b_n$ are the coefficients in a Fourier expansion of the isophote major-axis radius *a* expressed as a percent in the figure. Note that $a_4 > 0$ indicates disky-distorted isophotes and $a_4 < 0$ indicates boxy isophotes. We conclude that NGC 6166 becomes very boxy at large radii. The parameters $\Delta X_{\rm cen}$ and $\Delta Y_{\rm cen}$ measure the wandering of isophote center coordinates as functions of *a*.

Finally, as discussed further below, we use a major-axis, (0.″2-)two-pixel-wide cut profile to verify that the ellipse fitting was not adversely affected by the companion galaxies.

Seriously discrepant data in the profiles at small radii (usually because of inadequate spatial resolution) and at large radii (usually because of spatial variations in sky brightness) were pruned out before final averaging. Two additional complications require discussion.

1. Three additional cluster galaxies lie in projection close to the center of NGC 6166 (e.g., Minkowski [1961](#); Burbidge [1962](#); Tonry [1984](#), [1985](#)). Profile calculations need to correct for the light of these galaxies. Lauer ([1986](#); see also Lachièze-Rey et al. [1985](#)) decomposed the four galaxies using ground-based images and concluded that the two large companions are relatively undistorted, consistent with the hypothesis that they are not strongly interacting

with NGC 6166. It was already known that the brighter two companions differ in velocity from NGC 6166 by $-1520$ km s$^{-1}$ and $+570$ km s$^{-1}$ (e.g., Minkowski [1961](#)); these velocity differences are consistent with true separations that are similar to the projected ones, but they do not clearly establish a close physical relationship. We follow Lauer and assume that NGC 6166 itself is not affected by the companions. We therefore calculate its profile by masking out the companions.

2. There is patchy dust absorption near the galaxy center. We take this into account next.

Figure [8](#) illustrates both problems. The top image shows isophotes at average major-axis radii of 7.″9, 11.″7, 18.″6, and 24.″9. Above the center, all contours except the one at 24.″9 are substantially affected by the closest companion. Various strageties were used to correct for the companions. For some
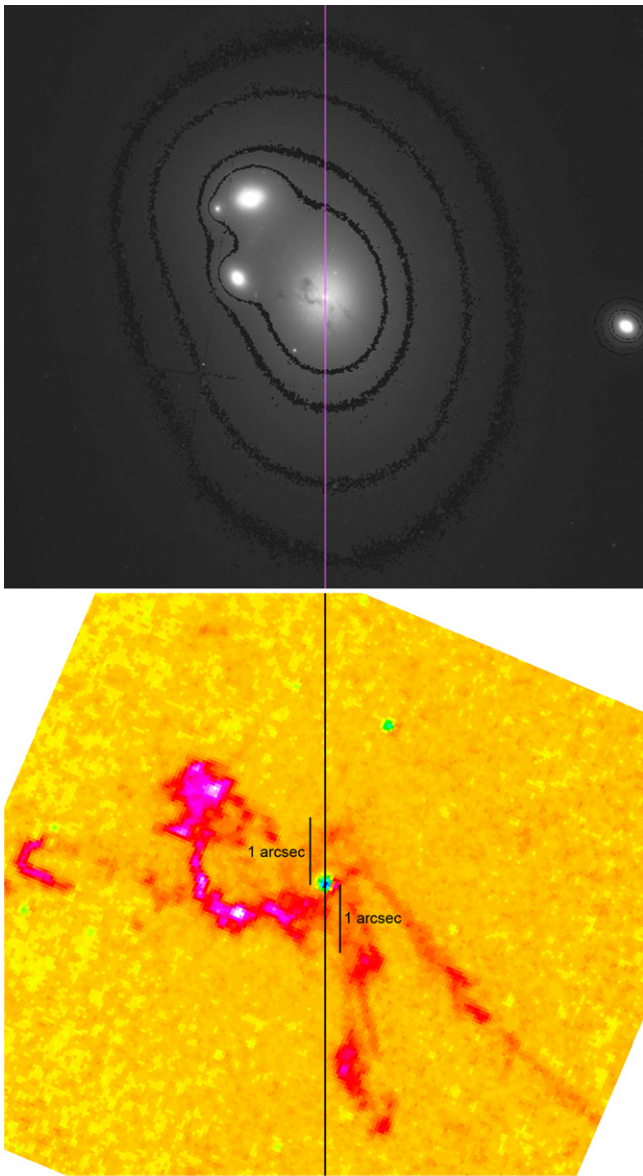
**Figure 8.** Central dust distribution in NGC 6166 shown (*top*) in the *HST* WFPC2 F555W *V*-band image and (*bottom*) by the ratio of an *HST* ACS F814W *I*-band image to an ACS F475W *g*-band image. The scale of the top image is $0\rlap{.}''1$ pixel$^{-1}$; the scale of the bottom image is $0\rlap{.}''05$ pixel$^{-1}$. Both images are rotated by $\Delta\mathrm{PA} = -23°$ so that the inner major axis is vertical (see Figure 1). In the bottom image, *g*- to *I*-band flux ratios $f_g/f_I$ are color coded as follows: yellow corresponds to $f_g/f_I = 1.0$; red corresponds to $f_g/f_I = 0.8$, and white corresponds to $f_g/f_I = 0.6$. The central blue pixel has $f_g/f_I \simeq 2.0$: the central source has at least some contribution from an AGN. Long vertical lines show the position of the two-pixel-wide, *V*-band cut profile measured in the top image. This image also includes four contour levels to show how companion galaxies affect the isophotes. We use only these parts of the cut profile that are as unaffected by companions as possible.

profiles, the companions were masked; for others, contaminated pixels were replaced by pixels from the opposite side of the galaxy center. The same strategy was used on the dust contamination; the most reliable results were obtained by interpolating through the dust in the right-hand quadrants and then replacing the most strongly affected pixels in the left quadrants by pixels from the opposite side of the center. All these procedures are somewhat vulnerable, because isophote fitting requires many pixels that need correction. So, as a check

on the isophote fitting, we derived a major-axis cut profile along the vertical line in Figure 8. The cut is 2 pixels $= 0\rlap{.}''2$ wide in the F555W WF image. The lower part of Figure 8 shows that the cut is minimally affected by dust (a few pixels were corrected). More importantly, we used pixels only from the bottom half of the image at radii where the top half is affected by the companions shown and only from the top half of the image at much larger radii where a companion not illustrated in the figure begins to be important.

Figure 9 shows that the average *V*-band composite profile is robustly determined. We have enough different data sets with different problems (e.g., non-flatness of the sky brightness) so that agreement among data sets reliably identifies problem points. They are pruned. Near the center, the profiles that are corrected with Lucy–Richardson deconvolution (Lucy 1974; Richardson 1972)—i.e., the ones from Lauer et al. (1995) and from the CFHT Cassegrain camera—agree with the much higher-resolution WF profile. In fact, since the *V*-band cut profile is most free of dust effects, it is used at radii near $1''$ in preference to the Lauer et al. (1995) data. (The difference is only a few hundredths of a mag arcsec$^{-2}$—see Figure 11.) Most important: *The major-axis cut profile agrees with the isophote fit profiles to $\lesssim 0.02\ V\,mag\,arcsec^{-2}$. The success of this check is important to our confidence in the final profile.*

The average *V*-band photometry is tabulated in Table 3.

### 3.3. Composite I-band Brightness Profile of NGC 6166

An *I*-band composite profile is derived in Figure 10, albeit from few sources. We need it primarily as another check of the *V*-band profile, including the ellipticity and position angle. The central profile and VEGAMAG zeropoint are from an *HST* ACS F814W image (GO program 9293; H. Ford, P. I.). It helps that dust is less important at *I* band. However, we can go further: the availability of an ACS F475W image (GO program 12238, W. Harris, P. I.) allows us to make a dust-corrected image, as follows.

First, the F475W *g*-band image was rotated and registered to $\sim$0.2 pixel accuracy with the F814W *I*-band image. Then a dust-corrected *I*-band image was derived using the procedure described in Nowak et al. (2008, Appendix A) and summarized here. In the following, $f_g$ and $f_I$ are the F475W and F814W surface fluxes per square arcsecond; no subscript indicates magnitudes or fluxes as observed, a subscript "0" refers to an extinction-corrected quantity. From the relation,

$$A_I \equiv I - I_0 = \alpha E(g - I), \qquad (2)$$

where $A_I$ is the *I* absorption and $E(g - I) \equiv (g - I) - (g - I)_0$ is the reddening in the color $(g - I)$, it follows that:
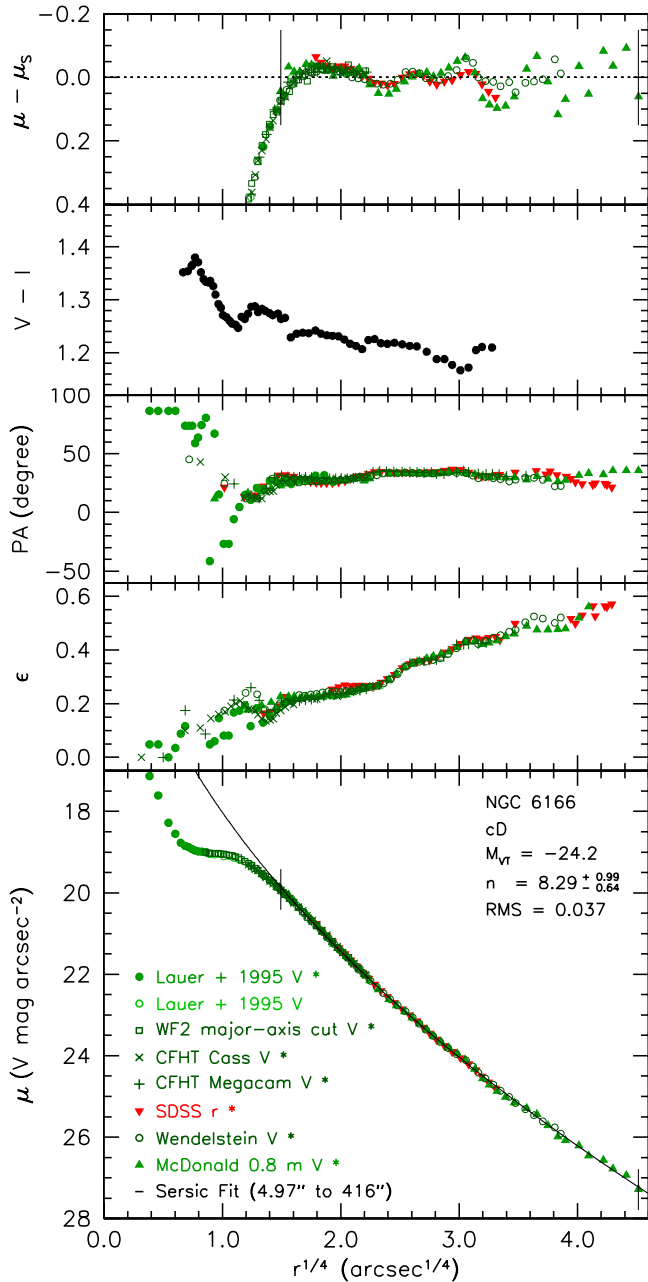
$$f_{I,0} = \frac{f_I^{\alpha+1}}{f_g^{\alpha}} \frac{f_{g,0}^{\alpha}}{f_{I,0}^{\alpha}}. \qquad (3)$$

If the stellar population gradient in the inner regions of NGC 6166 is negligible, then $f_{g,0}/f_{I,0} \approx$ constant and thus:

$$f_{I,0} \propto \frac{f_I^{\alpha+1}}{f_g^{\alpha}}. \qquad (4)$$

The parameter $\alpha$ is determined by

$$\alpha = \left(A_g/A_I - 1\right)^{-1} \approx 1.0, \qquad (5)$$

**Figure 9.** Major-axis profile measurements of NGC 6166: those labeled * in the key are used to calculate the average profile used in the analysis. The curve is a Sérsic fit in the radius range shown by the vertical dashes. The fit rms = 0.037 mag arcsec$^{-2}$; the residuals are shown in the top panel. The next panel downward shows the $V - I$ color profile via the $I$-band profile from the next section. The brightness profile shows no sign of two-component structure; i.e., the cD halo is not distinguishable using photometry alone.

where we have assumed a standard extinction curve to obtain the numerical value for the filters considered here (e.g., Savage & Mathis [1979]).

The correction is not perfect, because it is based on the assumption that all of the dust is in a screen in front of the image. In NGC 6166, most of the dust is near the middle of the galaxy, in front of only about half of the stars. Then Equation (5) overcorrects for the dust. Better results are obtained if we adopt a smaller value for $\alpha$ (a value of 0 would imply no correction). After some experimenting, we adopt

$\alpha = 0.6$, which yields the smoothest appearance of the isophotes. Explicitly,

$$f_{I,\text{dust-corrected}} = f_{I,\text{observed}}^{1.6}\big/f_{g,\text{observed}}^{1.6} \qquad (6)$$

The residual dust contamination is small.

Then the brown circles in Figure [10] are derived from the dust-corrected image using Bender's isophote fitting program. The red points are derived using VISTA profile on the dust-corrected image after 80 iterations of Lucy–Richardson deconvolution and after further cleaning of dust as discussed in Section [3.2]. These profiles agree essentially perfectly.

A final check is possible using an *HST* NICMOS2 F160W image (GO program 7453, J. Tonry, P. I.). There is no star in the field of view, so we do not attempt point-spread function (PSF) deconvolution. But dust is essentially unimportant. The core profile calculated from this image also agrees very well with the $I$-band results, when PSF blurring is taken into account. In particular, the F160W profile confirms that the core profile is cuspier at red wavelengths than it is in $V$ band.

### 3.4. Photometry Results. I. The Profile in the Core

Figure [11] illustrates our Section [3.3] conclusion: *The core profile of NGC 6166 is cuspier at red wavelengths than it is in V band. We suggest that the difference is caused by V-band absorption over the entire central arcsec of the galaxy*. Clear hints of widespread, low-level absorption are visible in Figure [8].

It is difficult to measure the power-law cusp slope far inside the profile break radius $r_b = 2\overset{''}{.}41$ (Lauer et al. [2007]). The reason is that the nuclear source is spatially resolved and has an unknown profile. Whether it consists of stars or an AGN or some combination, we cannot subtract it robustly. However, the shallowest $I$-band slope at $r \sim 0\overset{''}{.}5$ to $1\overset{''}{.}0$ corresponds to a Nuker function (Lauer et al. [1995]) $\gamma \simeq 0.13$. This agrees with $\gamma = 0.12$ obtained in Lauer et al. ([2007]; any correction for the nuclear source is not discussed). Previous estimates, $\gamma = 0.08$ (Lauer et al. [1995]) and $\gamma = 0.081$ (Byun et al. [1996]), were determined from the Lauer et al. ([1995]) $V$-band PC1 profile shown in Figure [11]. Our $V$-band cut profile is even flatter than Lauer's profile—it is less affected by *patchy* dust—so our composite $V$-band profile is even less cuspy than $\gamma \simeq 0.08$.

The cuspiness of the central profile affects no conclusions of this paper. But it will be important to use the appropriate, dust-free profile if in future we obtain stellar kinematic data that allow a dynamical search for a supermassive black hole.

### 3.5. Photometry Results. II. The cD Structure of NGC 6166 is Not Recognizable from the Shape of the Brightness Profile

Our profile measurements in Figures [9] and [10] do not show the two-component structure that is so obvious in Figure [6]. We believe that the Oemler ([1976]) profile is in error; the most likely reason is the difficulty of correcting for the many cluster galaxies that overlap the cD halo. Modern ellipse-fit software copes more robustly with incomplete isophotes.

A single Sérsic ([1968]) function fits the complete profile of NGC 6166 outside the cuspy core. Both this result and the Sérsic index, $n = 8.3_{-0.6}^{+1.0}$ in $V$ band or $7.8_{-1.0}^{+1.4}$ in $I$ band, are completely normal for core-boxy-nonrotating ellipticals.

**Table 3**
Major-axis *V*-band Brightness Profile of NGC 6166

| Radius (arcsec) | Brightness ($V$ mag arcsec$^{-2}$) | Ellipticity | PA (degrees) | Radius (arcsec) | Brightness ($V$ mag arcsec$^{-2}$) | Ellipticity | PA (degrees) |
|---|---|---|---|---|---|---|---|
| 0.022 | 17.132 | 0.000 | 86.5 | 10.48 | 20.813 | 0.225 | 28.4 |
| 0.044 | 17.608 | 0.000 | 86.5 | 11.62 | 20.954 | 0.231 | 28.2 |
| 0.088 | 18.279 | 0.000 | 86.5 | 12.75 | 21.083 | 0.236 | 27.0 |
| 0.132 | 18.550 | 0.035 | 86.5 | 13.84 | 21.205 | 0.236 | 27.5 |
| 0.176 | 18.771 | 0.088 | 80.2 | 14.94 | 21.314 | 0.231 | 28.5 |
| 0.220 | 18.846 | 0.130 | 73.8 | 16.21 | 21.436 | 0.236 | 27.9 |
| 0.264 | 18.879 | 0.120 | 59.5 | 17.85 | 21.577 | 0.242 | 28.2 |
| 0.308 | 18.928 | 0.120 | 73.8 | 19.65 | 21.727 | 0.247 | 28.9 |
| 0.352 | 18.961 | 0.120 | 59.0 | 21.60 | 21.870 | 0.253 | 29.9 |
| 0.400 | 18.981 | 0.120 | 63.8 | 23.73 | 22.015 | 0.258 | 29.5 |
| 0.460 | 18.988 | 0.110 | 58.7 | 25.56 | 22.156 | 0.262 | 31.3 |
| 0.550 | 19.004 | 0.087 | 80.6 | 28.56 | 22.343 | 0.267 | 33.6 |
| 0.628 | 19.021 | 0.092 | 66.9 | 31.05 | 22.462 | 0.280 | 34.1 |
| 0.671 | 19.036 | 0.096 | 53.2 | 33.88 | 22.613 | 0.294 | 33.9 |
| 0.773 | 19.031 | 0.060 | 39.4 | 37.56 | 22.764 | 0.311 | 33.5 |
| 0.873 | 19.033 | 0.153 | 15.3 | 41.83 | 22.914 | 0.335 | 33.9 |
| 0.951 | 19.043 | 0.140 | 7.1 | 46.03 | 23.062 | 0.350 | 33.8 |
| 1.05 | 19.049 | 0.127 | −1.1 | 50.44 | 23.212 | 0.357 | 33.6 |
| 1.15 | 19.063 | 0.170 | 30.0 | 55.05 | 23.363 | 0.362 | 33.4 |
| 1.25 | 19.075 | 0.081 | 23.1 | 59.84 | 23.512 | 0.368 | 33.3 |
| 1.38 | 19.087 | 0.190 | 16.2 | 65.39 | 23.660 | 0.376 | 33.3 |
| 1.52 | 19.115 | 0.194 | 9.3 | 71.78 | 23.807 | 0.389 | 34.2 |
| 1.67 | 19.138 | 0.174 | 4.6 | 78.98 | 23.954 | 0.412 | 34.1 |
| 1.82 | 19.188 | 0.210 | 8.9 | 87.10 | 24.102 | 0.426 | 34.1 |
| 2.02 | 19.228 | 0.210 | 13.3 | 95.39 | 24.296 | 0.434 | 32.0 |
| 2.23 | 19.290 | 0.179 | 15.7 | 104.15 | 24.509 | 0.425 | 31.2 |
| 2.40 | 19.338 | 0.185 | 12.9 | 114.68 | 24.712 | 0.435 | 30.5 |
| 2.65 | 19.405 | 0.174 | 12.1 | 123.74 | 24.864 | 0.445 | 30.2 |
| 2.90 | 19.460 | 0.197 | 14.2 | 134.90 | 25.015 | 0.460 | 28.8 |
| 3.20 | 19.539 | 0.155 | 16.6 | 145.38 | 25.158 | 0.468 | 28.8 |
| 3.51 | 19.615 | 0.160 | 19.0 | 161.62 | 25.301 | 0.496 | 29.5 |
| 3.85 | 19.696 | 0.166 | 21.8 | 180.58 | 25.501 | 0.506 | 29.4 |
| 4.22 | 19.771 | 0.162 | 25.5 | 198.02 | 25.714 | 0.475 | 28.7 |
| 4.53 | 19.847 | 0.171 | 24.7 | 216.11 | 25.884 | 0.500 | 28.1 |
| 4.98 | 19.924 | 0.202 | 27.4 | 231.21 | 26.075 | 0.479 | 27.5 |
| 5.49 | 20.037 | 0.197 | 27.4 | 259.42 | 26.204 | 0.520 | 31.6 |
| 5.95 | 20.101 | 0.213 | 27.1 | 280.87 | 26.453 | 0.561 | 33.3 |
| 6.59 | 20.228 | 0.211 | 27.0 | 316.96 | 26.567 | 0.561 | 32.4 |
| 7.38 | 20.364 | 0.219 | 27.9 | 341.98 | 26.773 | 0.561 | 35.7 |
| 8.06 | 20.473 | 0.223 | 27.9 | 379.32 | 26.935 | 0.561 | 35.7 |
| 8.58 | 20.551 | 0.220 | 28.4 | 415.72 | 27.283 | 0.561 | 35.7 |
| 9.47 | 20.678 | 0.223 | 27.9 | ... | ... | ... | ... |

Figure 12 compares NGC 6166's profile shape with the sample of elliptical galaxies studied by KFCB. They found that *n* ranges from 5.4 ± 0.3 to 9 ± 1 for their core ellipticals (red profiles in Figure 12). NGC 6166 is virtually indistinguishable from these galaxies; indeed, many core ellipticals have shallower outer profiles log $I(r/r_b)$ than does NGC 6166. It is especially interesting to contrast NGC 6166 with M87. M87 is by all arguments a more marginal cD than NGC 6166. But a Sérsic fit to its overall profile gives $n = 12^{+2}_{-1}$, larger than $n \simeq 8$ in NGC 6166. Plausible allowance for a cD halo in M87—i.e., exclusion of the outermost profile points—gave a marginally better fit with $n = 9^{+2}_{-1}$, consistent with our fit to NGC 6166 but with only a little extra light in the cD halo of M87. Such a halo is less—not more—obvious in NGC 6166.

A two-component, Sérsic–Sérsic decomposition is allowed by our data (Section 4), but the fit is not significantly better than the one-component decomposition. There is no reason to believe that we detect two components from photometry alone.

This is a surprising result. We plan but have not yet carried out similar photometry of other cD galaxies. We therefore do not know that the present results on NGC 6166 apply more generally to all cD galaxies. Nevertheless:

We arrive at an ironic situation: *The spectroscopy results resoundingly confirm our standard picture that the cD galaxy NGC 6166 in Abell 2199 has an outer halo that consists of debris from member galaxies. The halo stars are dynamically controlled by the cluster, not the central galaxy, and they have the kinematics (i.e., more nearly the systemic velocity and the velocity dispersion) of the other galaxies in the cluster, even when the cD is dynamically colder and in motion with respect to the sea of background stars. But the supposedly much easier task of recognizing the presence of a cD halo from two-component structure in the surface brightness distribution turns out to fail dramatically in the nearest, most prototypical cD galaxy, NGC 6166.*
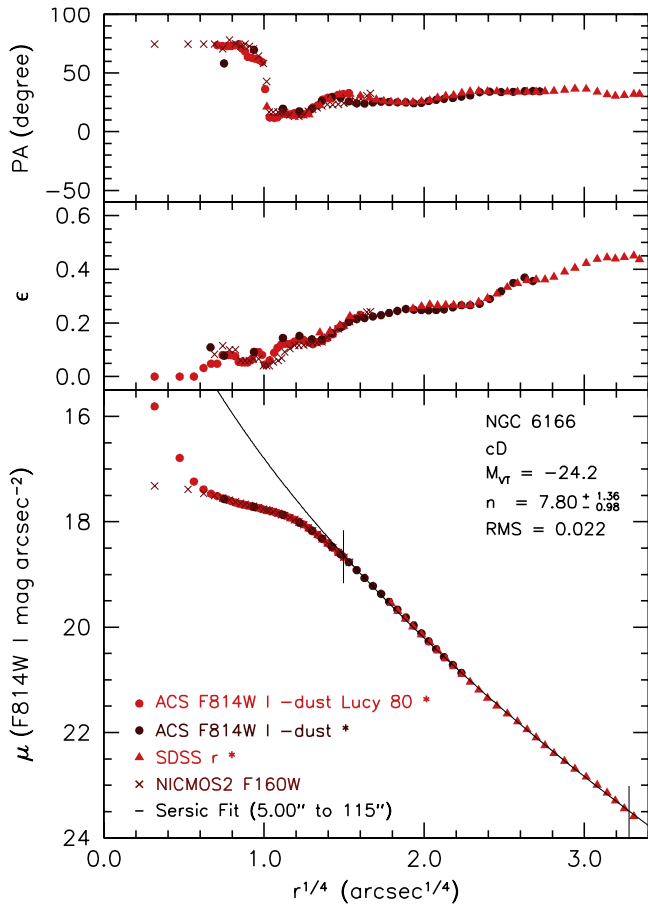
**Figure 10.** Major-axis *I*-band profile measurements of NGC 6166. Profiles labeled * are averaged to make the mean profile used in the analysis. The curve is a Sérsic fit in the radius range shown by the vertical dashes; the fit rms = 0.022 mag arcsec$^{-2}$. Again, there is no sign of two-component structure: the cD halo is not distinguishable via photometry alone.

**Figure 11.** Major-axis *V*- and *I*-band profiles of NGC 6166 fitted together outside the core ($V - I = 1.24$). Both Sérsic fits are also shown. The purpose of this figure is to show that the core profile is robustly cuspier in *I* band than in *V* band. This is probably due to dust absorption in *V* band in the central $r \sim 1''$, as suggested also by Figure 8. It is not due to PSF smearing; even 80 iterations of Lucy–Richardson deconvolution have essentially no effect on the shallow core profile. Also supporting our interpretation is the observation that an F160W *HST* NICMOS2 profile agrees with the *I*-band data as well as can be expected, given PSF blurring. The difference between the *V* and *I* core profiles affects no conclusions of this paper, but it should be kept in mind in making dynamical models to look for any central supermassive black hole.
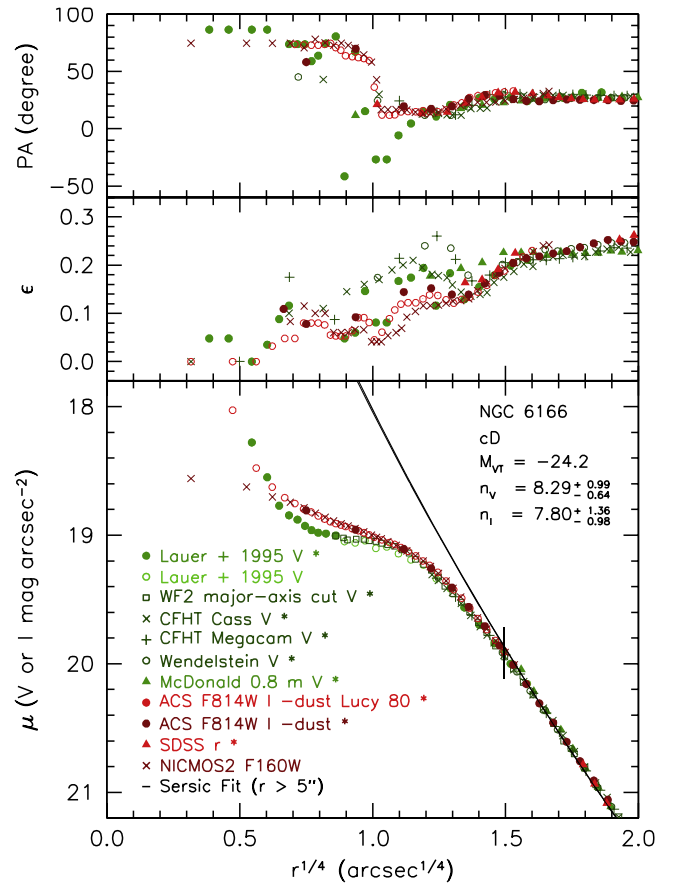
### 3.6. Photometry Results. III. Recognizing NGC 6166 as a cD Galaxy via Quantitative Differences in Structural Parameters

Is it possible to recognize cD galaxies by photometry alone? A photometric technique is desirable, because spectroscopy to look for an outward rise in velocity dispersion is expensive. Our results suggest a partial answer: The cD nature of NGC 6166 can be recognized via quantitative differences in structural parameters and parameter correlations. This helps but is not entirely satisfactory. Parameter distributions for cD galaxies and non-cD ellipticals overlap. There may be physics in this. The physical differences between cDs and core-boxy-nonrotating ellipticals may be smaller than we have thought. Figures 13 and 14 illustrate these points.

Figure 13 compares the brightness profile of NGC 6166 to the Virgo cluster elliptical galaxies. Radii are plotted in kpc. NGC 6166 has a larger and fainter core than any elliptical in Virgo, including M87. And its outer profile is shallower and it reaches larger radii than that of any elliptical in Virgo, including M87. Quantitatively, the extreme cD NGC 6166 is distinguishable from normal core ellipticals. However, the marginal cD M87 (see KFCB) overlaps with other core ellipticals in its profile properties.

Figure 14 compares the structural parameters of NGC 6166 with parameter correlations from KFCB and from Kormendy & Bender (2012). These are projections of the "fundamental

plane" correlations (Djorgovski & Davis 1987; Dressler et al. 1987; Faber et al. 1987; Djorgovski et al. 1988; Djorgovski 1992; Bender et al. 1992, 1993), between the effective radius $r_e$ that encloses half of the light of the galaxy, the effective brightness $\mu_e$ at $r_e$, and (in this case) total absolute magnitude.

NGC 6166 parameters are based on an assumed distance of $D = 130.8$ Mpc (NASA/IPAC Extragalactic Database "NED" $D$(Local Group) for cluster Abell 2199 and the *WMAP* five-year cosmology parameters, Komatsu et al. 2009). NGC 6166 is plotted twice in Figure 14:

To get the less extreme point, we integrate the brightness and ellipticity profiles (that is, the two-dimensional isophotes) to the outermost data point in Figure 9, i.e., $r = 416''$ where $\mu_V = 27.28$ *V* mag arcsec$^{-2}$. This gives $V = 11.75$, $M_V = -23.86$, $r_e = 71''.2 = 45.2$ kpc, and $\mu_e = 23.76$ *V* mag arcsec$^{-2}$. Galactic absorption corrections are from Schlegel et al. (1998). This point in Figure 14 is consistent with a slight extrapolation to higher luminosity of the correlations for other ellipticals.

The more extreme point is derived by extending the profile to $r \simeq 2000'' \sim 1.3$ Mpc using the overall Sérsic fit and
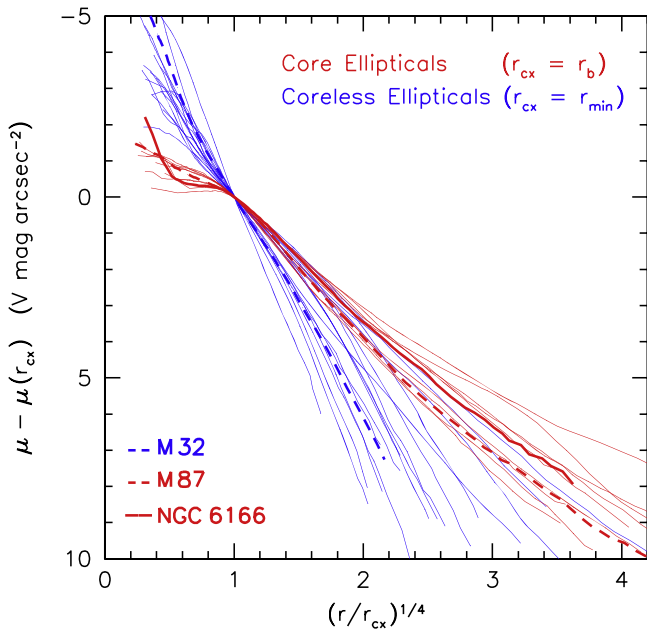
**Figure 12.** Major-axis profiles of all KFCB elliptical galaxies scaled together in radius and surface brightness. Core ellipticals are scaled at $r_{cx} = r_b$, the break radius given by the Nuker function fit in Lauer et al. (2007). Coreless ellipticals are scaled at the minimum radius $r_{min}$ that was used in the KFCB Sérsic fits; inside this radius, the profile is dominated by extra light above the inward extrapolation of the outer Sérsic fit. NGC 6166 and the fiducial galaxies M87 and M32 are plotted with thick lines. There is no sign of two-component structure in NGC 6166; its profile resembles those of other core galaxies. That is, the cD halo is not distinguishable using photometry alone.
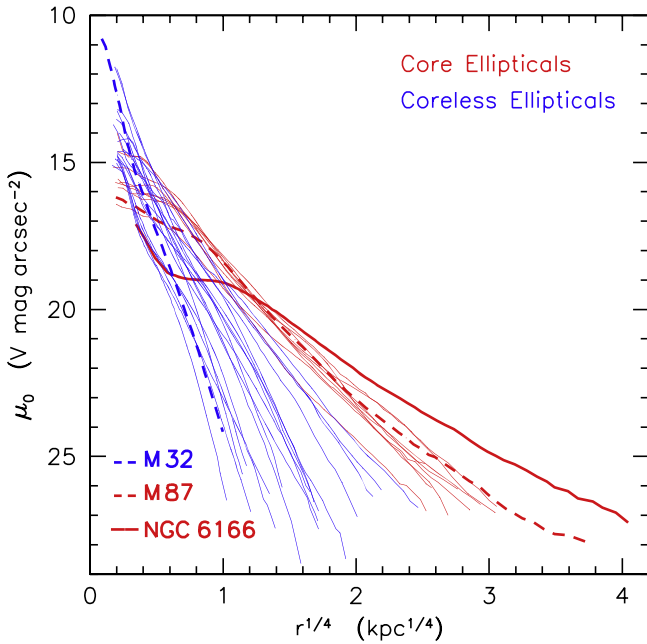


**Figure 13.** Major-axis profiles of all KFCB elliptical galaxies scaled so that radius is in kpc. The brightness profiles are corrected for Galactic absorption as in Schlegel et al. (1998). NGC 6166 is added; it and the fiducial galaxies M87 and M 32 are plotted with thick lines. NGC 6166 is not distinguished from the other galaxies by profile shape, but its parameters are extreme. That is, the cD halo is distinguishable quantitatively via the shallow outer profile and the consequently large effective radius.
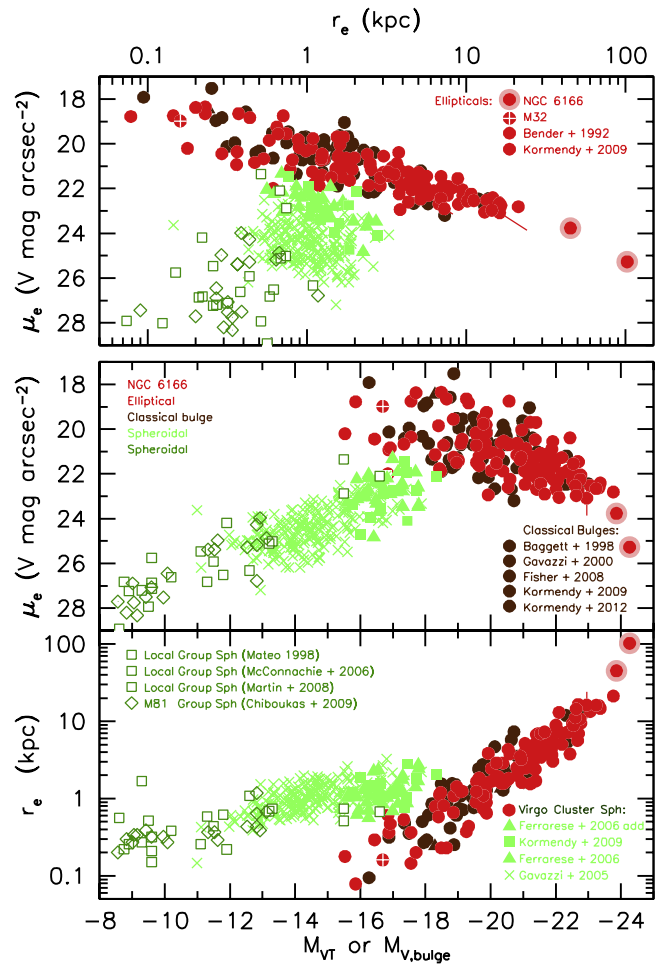


**Figure 14.** Structural parameter correlations for elliptical and spheroidal galaxies. Major-axis effective radii $r_e$ and effective surface brightnesses $\mu_e \equiv \mu(r_e)$ are calculated by integrating isophotes with the observed brightness and ellipticity profiles out to half of the total luminosity. S- and S0-galaxy bulge parameters are from Sérsic–Sérsic or (when appropriate) Sérsic-exponential photometric decompositions into bulge and disk components. The galaxy sample is from KFCB and from Kormendy & Bender (2012). When necessary, mean-axis parameters are corrected to the major axis. NGC 6166 is plotted twice; the smaller-$r_e$ point is for the integral of the surface brightness distribution out to the last data point in Table 3. To derive the outer point, the observed profile is extended to 30.9 $V$ mag arcsec$^{-2}$ using the Sérsic fit and keeping the ellipticity fixed at the value at the largest radii observed. Again, the cD nature of NGC 6166 together with its cluster-sized halo is evident quantitatively from the structural parameters.

keeping the outer ellipticity constant at the last observed value. The limiting surface brightness is 30.9 $V$ mag arcsec$^{-2}$; this is an "integration to infinity" similar to those discussed in KFCB. Then $V_T = 11.35$, $M_{VT} = -24.27$, $r_e = 162'' = 103$ kpc, and $\mu_e = 25.27$ $V$ mag arcsec$^{-2}$. Within the scatter, this point is consistent with a larger extrapolation of the correlations for normal ellipticals. It deviates slightly from linear correlations in having larger $r_e$ and fainter $\mu_e$, but slightly curved fits to normal ellipticals would not show NGC 6166 as deviant.

We conclude that NGC 6166 is more extreme than the ellipticals in the combined sample in Figure 14 in the sense expected for a cD: it has larger effective radius and fainter effective brightness. In this sense, the cD structure is recognizable quantitatively in the parameter correlations.

cD and non-cD galaxies overlap in parameter distributions (Schombert 1986, 1987). And yet, the cD NGC 6166 is
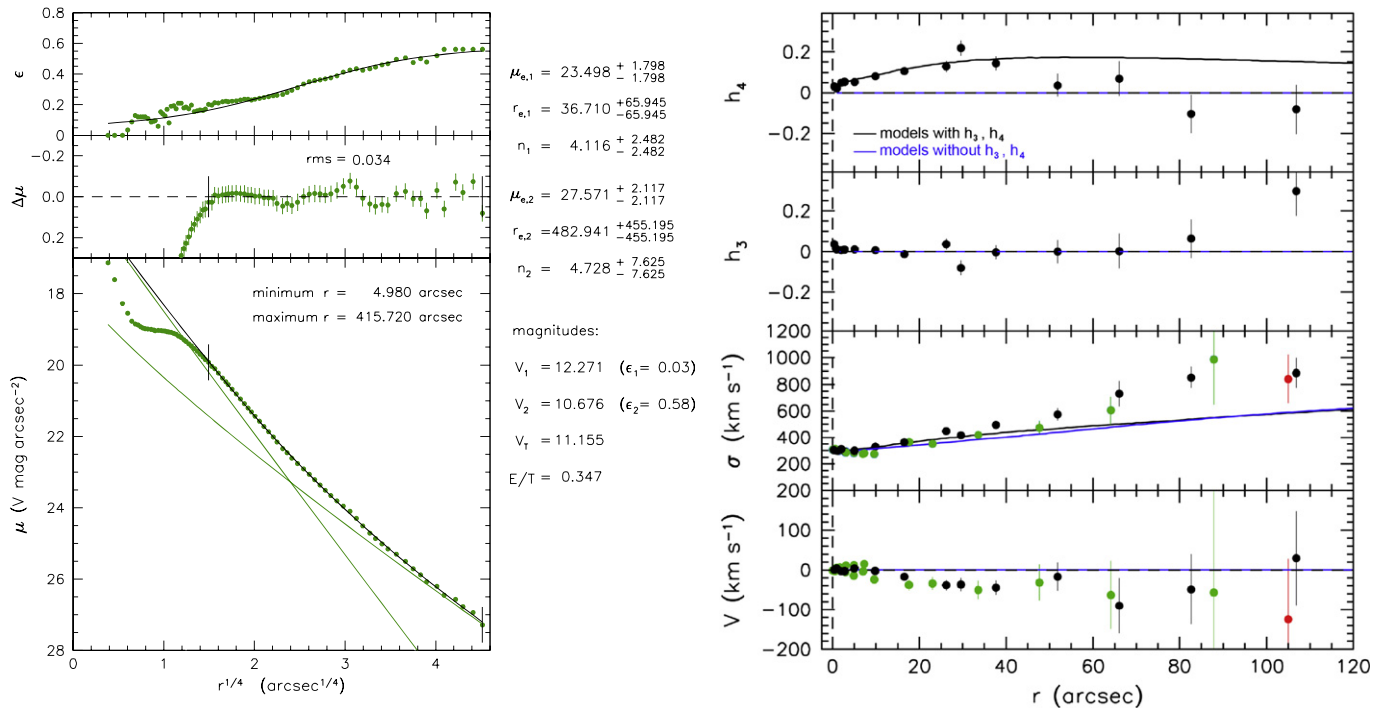
**Figure 15.** (*Left 3 panels*) minimum-$\chi^2$ decomposition of the averaged major-axis *V*-band brightness profile of NGC 6166 into two Sérsic functions. Parameters are given in the keys. Component 1 is the central galaxy; Component 2 is an initial estimate of the cD halo. If each component has constant ellipticity as given in the key, then the implied composite (*black curve in the top panel*) has approximately the correct observed ellipticity profile (*green points in the top panel*). This gives the total magnitude $V_1$ and $V_2$ of each component and the total magnitude $V_T$ of the galaxy as extrapolated to infinite radius. (*Right 4 panels*) the points show velocity $V$, velocity dispersion $\sigma$, and Gauss–Hermite coefficients $h_3$ and $h_4$ of the line-of-sight velocity distribution. These are the measurements presented in Section 2. The blue and black curves show predicted values given by the decompostion in the left panels if Component 1 has $\sigma = 300$ km s$^{-1}$ and Component 2 has $\sigma = 865$ km s$^{-1}$. The decomposition does not fit the data—the component Sérsic indices are too large; i.e., the components overlap too much in radius, so $\sigma$ rises too slowly toward the cluster dispersion. Note that $r^{1/4} = (110 \text{ arcsec})^{1/4} = 3.24$ in the left panels.

qualitatively different from non-cD ellipticals, even brightest cluster galaxies. This is important, because cD and brightest cluster galaxies are often considered to be equivalent. But NGC 6166 is surrounded by an immense halo of stars that are controlled dynamically by the cluster potential, not by the central galaxy. Isolated ellipticals cannot have such halos, and observations of velocity dispersion profiles in non-cD core ellipticals show no rise in $\sigma$ at large radii (e.g., Kronawitter et al. 2000; Proctor et al. 2009; Weijmans et al. 2009; Foster et al. 2011; Raskutti et al. 2014).

We conclude (1) that cD structure is real and distinct from non-cD ellipticals but (2) that it is difficult to recognize the difference photometrically. Extreme structural parameters help (Figure 14). But in less extreme cases—and, to be certain, even in NGC 6166—velocity dispersion data are required to identify cluster halos reliably. The fact that cD classification is difficult is our problem, not the galaxy's.

## 4. PHOTOMETRIC AND KINEMATIC DECOMPOSITION OF NGC 6166 INTO AN ELLIPTICAL GALAXY PLUS A cD HALO

This section presents a decomposition of the inner, E-galaxy part of NGC 6166 and its cD halo that accounts for both the photometry and the velocity dispersion profile of the galaxy.

The best-fit two-component Sérsic–Sérsic decomposition is illustrated in the left part of Figure 15. We emphasize: the rms deviations $0.034\,V$ mag arcsec$^{-2}$ of the profile from the fit within the fit range (*vertical dashes across the $\mu$ and $\Delta\mu$ profiles*) are not significantly better than the deviations (Figure 9 rms = $0.037\,V$ mag arcsec$^{-2}$) of a single-Sérsic fit.

The decomposition in Figure 15 is similar to those in Huang et al. (2013a, 2013b)—it minimizes $\chi^2$ for two Sérsic components. Huang and collaborators interpret such decompositions as supporting a two-phase scenario of elliptical galaxy formation (Oser et al. 2010; Johansson et al. 2012) in which wet mergers rapidly build high-$z$, compact "red nuggets" (Buitrago et al. 2008; van Dokkum et al. 2010; Papovich et al. 2012; Szomoru et al. 2012) that later grow high-Sérsic-index halos via minor mergers. The inner component(s) in the decomposition are interpreted as descendent(s) of the red nuggets, and the outer component is interpreted as a later-accreted debris halo. Such a picture may be correct. But (1) it is not compellingly supported by the conclusion that two components fit the data better than one, and more importantly, (2) NGC 6166, with its cD halo, is a clearcut example of essentially the above processes, and in it, a two-component decomposition made by minimizing $\chi^2$ fails to explain the kinematics. As follows:

The observed dispersion profile implies that the central galaxy contributes most of the light along the line of sight out to $r \simeq 50'' \sim 32$ kpc ($D = 130.8$ Mpc). The brightness profile extends out to $r \simeq 416'' \simeq 260$ kpc in the cD halo. In the transition region, we look through a short line of sight through the galaxy and a long line of sight through the halo. This suggests a simple procedure to capture the essence of the $\sigma(r)$ profile. We assume that the components have independent Gaussian LOSVDs. To keep things simple, we assume that the galaxy has the brightness profile of Component 1 in Figure 15 and that it has $\sigma \sim 300$ km s$^{-1}$ at all radii. We assume that the cD halo has the brightness profile of Component 2 and
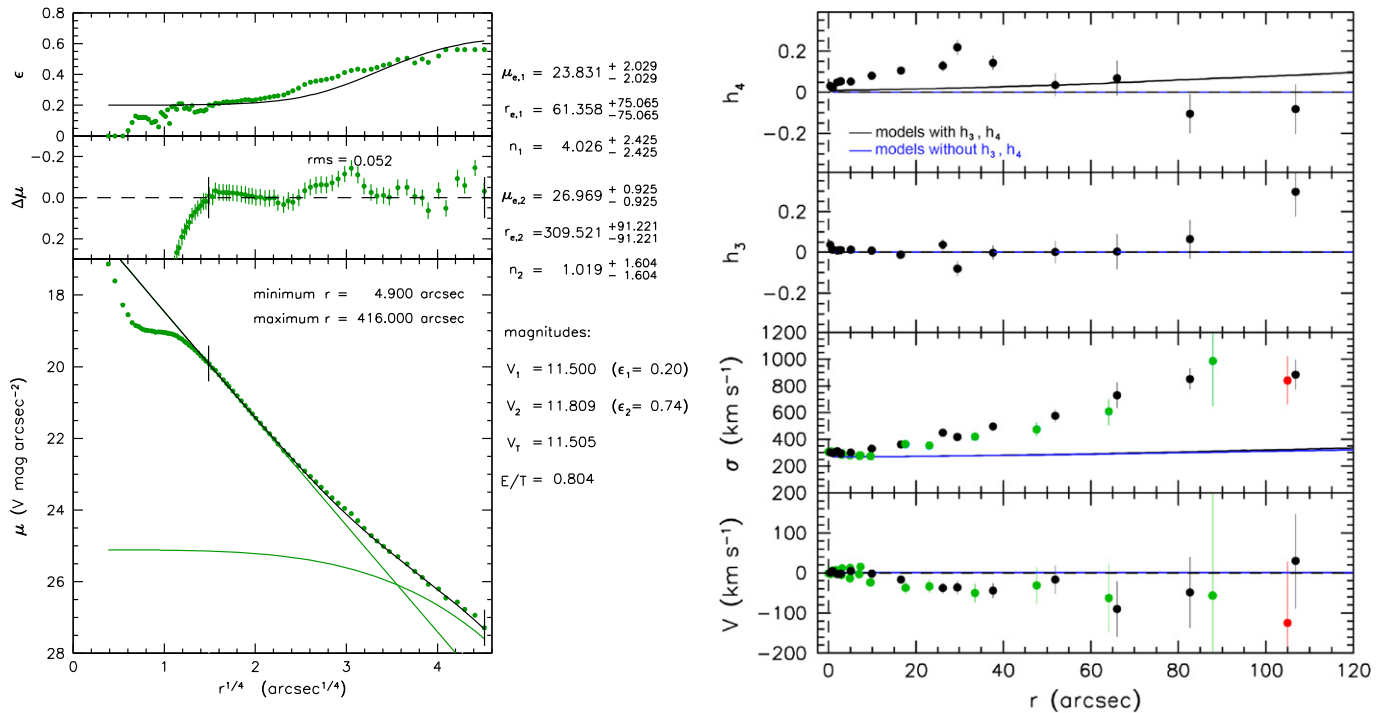
**Figure 16.** (*Left 3 panels*) alternative decomposition of the major-axis *V*-band brightness profile of NGC 6166 into a Sérsic function main body and an exponential halo that is constrained to have a central surface brightness of 25 *V* mag arcsec$^{-2}$. Parameters are given in the keys. If each component has constant ellipticity (*see the key*), then the implied composite (*black curve in the top panel*) is a fairly poor fit to the observed ellipticity profile (*green points in the top panel*), not as good a fit as in Figure 15. The profile decomposition remains good, with rms = 0.052 mag arcsec$^{-2}$. Such Sérsic–exponential decompositions have gained some popularity as descriptions of cD galaxies. (*Right 4 panels*) from Section 2, the points show velocity *V*, velocity dispersion $\sigma$, and Gauss–Hermite coefficients $h_3$ and $h_4$ of the line-of-sight velocity distribution. The blue and black curves show predicted values given by the decomposition in the left panels if Component 1 has $\sigma = 300$ km s$^{-1}$ and Component 2 has $\sigma = 865$ km s$^{-1}$. Although the photometric decomposition looks good, the implied kinematics completely fail to fit the dispersion profile, because the main body of the galaxy dominates at $r^{1/4} = (110 \text{ arcsec})^{1/4} = 3.24$.

$\sigma \sim 865$ km s$^{-1}$ at all radii. This is an oversimplification. But if the decomposition in Figure 15 is approximately correct, then it should approximately fit the dispersion profile. It fails. The components overlap too much in radius; i.e., the inner component contributes too much light at large radii for the dispersion profile to increase outward as quickly as we observe toward $\sigma \sim 850$ km s$^{-1}$. Modifying the assumed inner and outer dispersions does not help.

*So a two-Sérsic-component photometric decomposition that minimizes $\chi^2$ fails to explain the velocity dispersion profile of NGC 6166. This argues for caution in the increasingly popular practice of making minimum-$\chi^2$, Sérsic–Sérsic decompositions of elliptical galaxies based on photometry alone. It does not work in NGC 6166, where the $\sigma(r)$ profile provides physically motivated guidance in how to interpret the results. This does not argue for confidence in decompositions of giant-boxy-coreless ellipticals that are well fit by single Sérsic functions and in which monotonically decreasing $\sigma(r)$ profiles provide no guidance about which decompositions measure something that is physically meaningful.*

Figure 16 tries a different kind of photometric decomposition that has been used to estimate the properties of cD halos. Seigar et al. (2007) and Donzelli et al. (2011) fit cD halos with exponential profiles. Since NGC 6166 is well fitted by a single Sérsic function, a Sérsic–exponential decomposition has a larger $\chi^2$ with respect to the photometric observations. It is therefore necessary to apply some additional constraint to force the program to find an exponential halo. We tried various decompositions in which the central surface brightness was constrained. All such decompositions behave similarly if we

require that the rms of the fit be consistent with measurement errors. Figure 16 shows an example in which the exponential is forced to have a central surface brightness of 25 *V* mag arcsec$^{-2}$. The fit rms = 0.052 *V* mag arcsec$^{-2}$ is worse than rms = 0.037 *V* mag arcsec$^{-2}$ in Figure 9 but is not excluded by the data. However, this halo is much too faint. The main galaxy contributes essentially all the light at radii where we have kinematic data, so the dispersion profile fails to rise significantly toward the outer observed value.

*Again, we conclude that Sérsic–exponential decompositions of cD galaxies—at least in the case of NGC 6166—are not well constrained physically using photometry alone.*

The "cure" is to make the two components be as separate as possible by decreasing both Sérsic indices. The resulting best fit gets worse—gets, in fact, increasingly *inconsistent* with the photometric measurement errors—but the fit to the dispersion profile gets better. Figure 17 shows the decompositions (two of many that we tried) that best fit $\sigma(r)$. Given the crude assumptions, it makes no sense to look for further improvement; the way to get a better fit is to make a full Schwarzschild (1979, 1982) model of the photometry and the kinematics. We save this exercise for a future paper. Here, we conclude from Figure 17 that NGC 6166 and its cD halo overlap less strongly in radius than a minimum-$\chi^2$ photometric decomposition (Figure 15) suggests.

Figure 17 shows that, to fit the $\sigma(r)$ profile of NGC 6166, we need to make a photometric decomposition that does not minimize $\chi^2$. This is no disaster: we chose Sérsic functions for each component, and our experience that they fit non-cD ellipticals well (KFCB) may not be relevant here.
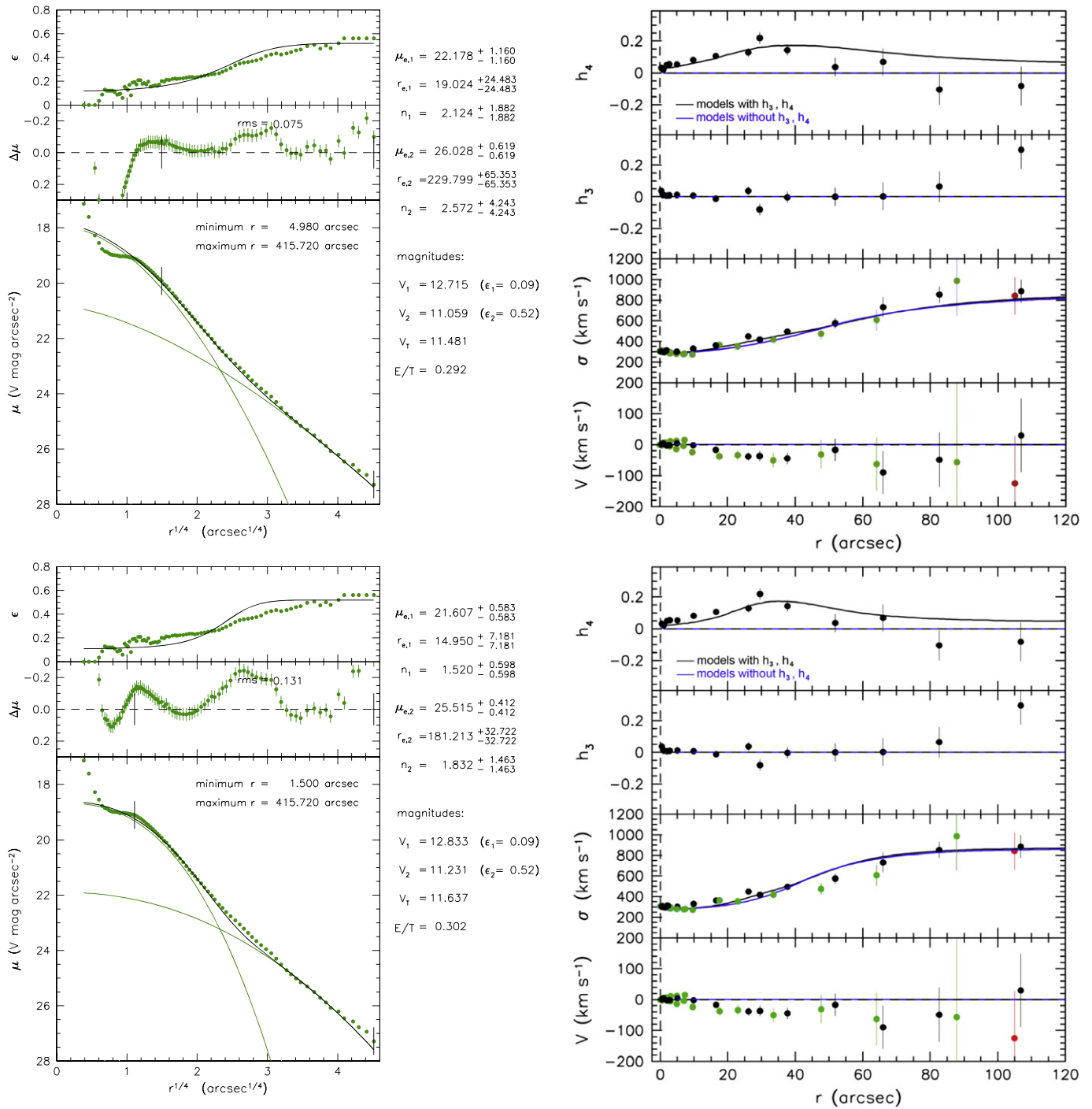
**Figure 17.** Two similarly acceptable photometric (*left panels*) and kinematic (*right panels*) decompositions of NGC 6166 into a main body and a cD halo. (*Left 3 panels*) photometric decomposition of the major-axis *V*-band brightness profile of NGC 6166 into two Sérsic functions. The components are constrained to have small Sérsic indices so that they overlap less strongly in radius than in Figure 15. The bottom decomposition uses smaller Sérsic indices than the top decomposition. Parameters are given in the keys. Component 1 is the central galaxy; Component 2 is the estimate of the cD halo. If each component is has constant ellipticity (*see the key*), then the implied composite (*black curve in the top panel*) is a somewhat poor fit (*top decomposition*) or a very poor fit (*bottom decomposition*) to the observed ellipticity profile (*green points in the top panel*). Also, the overall fit rms = 0.075 *V* mag arcsec$^{-2}$ (*top*) and 0.131 *V* mag arcsec$^{-2}$ (*bottom*) are substantially worse than rms = 0.037 *V* mag arcsec$^{-2}$ of the single-Sérsic fit in Figure 9. Instructed to minimize $\chi^2$, the program does not want such small Sérsic indices. The total magnitude $V_1$ and $V_2$ of each component and the total magnitude $V_T$ of the galaxy are given in the key. (*Right 4 panels*) From Section 2, the points show velocity *V*, velocity dispersion $\sigma$, and Gauss–Hermite coefficients $h_3$ and $h_4$ of the line-of-sight velocity distribution. The black and blue curves show predicted values given by the photometric decomposition if Component 1 has $\sigma = 300$ km s$^{-1}$ and Component 2 has $\sigma = 865$ km s$^{-1}$. These two decompositions were chosen from many that we tried because they fit the dispersion data reasonably well. At $r^{1/4} = (110 \text{ arcsec})^{1/4} = 3.24$, the cD halo dominates completely.

Support for our photometric + kinematic decomposition is provided by the result in Figures 15 and 17 that the predicted $h_4 > 0$ agrees with the observations at radii $r \lesssim 40''$. At larger radii, the predicted $h_4$ remains positive but trends toward zero. The spectra there are too noisy to provide reliable constraints.

17

Figures 15–17 suggest that the main body of NGC 6166 contains $\sim30\% \pm 2\%$ and the cD halo contains $\sim70\% \pm 2\%$ of the total luminosity. The formal error is probably an underestimate.

For the assumptions made in Section 3.6 to get total absolute magnitudes of $M_{VT} = -23.86$ out to the last photometric data point or $-24.27$ extrapolated to infinity, the main body of NGC 6166 has $M_V \simeq -22.6$ or $-23.0$. These are essentially identical to the absolute magnitudes of M87 and NGC 4472 in the Virgo cluster (KFCB). The cD halo of NGC 6166 has $M_V \simeq -23.5$ or $-23.9$, i.e., 0.3–0.6 mag brighter than the brightest galaxy in the Virgo cluster.

(NB: if we interpret the total profile as the sum of several components as in Figures 15–17, then the Sérsic index of each component is smaller than $n \simeq 8.3$ for the single-component fit in Figure 9. In Figure 15, the inner component has $n = 4.1$; the outer component has $n = 4.7$. Increasing the number of components forces $n$ to be smaller. The extreme version is multi-Gaussian decomposition (Emsellem et al. 1994; Cappellari 2002): when the number of components is very large, then $n$ must be very small. A Gaussian $n = 0.5$ is convenient for numerical reasons. Such decompositions are useful, precise representations of the profile, as long as no physical significance is attached to individual components.)

## 5. SPHERICAL JEANS MODELS

Our kinematic measurements allow a detailed study of the velocity distribution of the galaxy plus stellar halo and of the total mass distribution including X-ray gas and dark matter. Orbit-superposition models (Schwarzschild 1979, 1982) are postponed to a future paper. Here, we explore the stellar velocity anisotropy using spherical Jeans models.

Figures 18 and 19 show results for Jeans-model fits to our photometry and $\sigma$ data. We assume that dark matter ("DM," including X-ray gas) is distributed as a non-singular pseudo-isothermal $\rho \propto (1 + r^2/r_c^2)^{-1}$ (Kormendy & Freeman 2015) or as an NFW density profile (Navarro et al. 1996, 1997). We choose the outer, circular-orbit rotation velocity $V_{circ} = 1160$ km s$^{-1}$ of massless test particles in the halo to be consistent with the cluster dispersion of $819 \pm 32$ km s$^{-1}$. Next, we assume that the stars have a Kroupa (2001) initial mass function with mass-to-light ratio $M/L_V = 4$, based on the metallicity and age estimated in the next section and on stellar population models of Maraston et al. (2003). Then the only free parameter left is the scale length $r_s$ of the NFW profile or the core radius $r_c$ of the isothermal. We vary this scale length until the mass density profile matches the one derived from the X-ray gas by Markevitch et al. (1999). In this way, we derive a density profile over the full radius range (Figure 19) without yet using our kinematic data on NGC 6166. Finally, we vary the velocity anisotropy as a function of radius (*middle panel* of Figure 18) until we reproduce the observed velocity dispersion profile (*bottom panel* of Figure 18). Although the isothermal sphere and the NFW DM profiles are quite different, especially at $r \leqslant 16$ kpc, the anisotropy profiles are qualitatively similar. That is, the total density profile and the dispersion profile together determine the anisotropy profile.

The important result is observed at radii $r \sim 20''$–$70''$, where $\sigma$ rises from the galaxy value of 300 km s$^{-1}$ to the cluster value of >800 km s$^{-1}$. In this radius range, the tangential velocity dispersion is larger than the radial one, $\sigma_t > \sigma_r$. We were unable to change this result by varying the DM profile. The
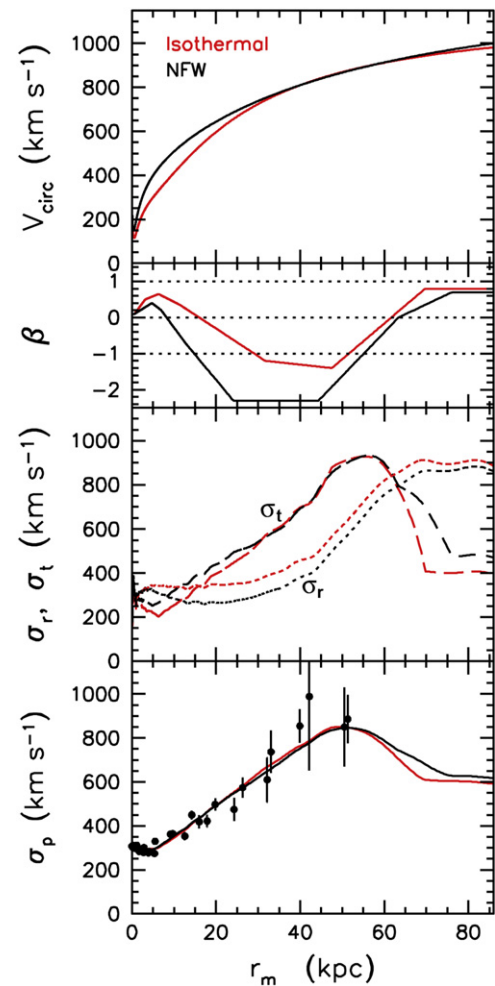


**Figure 18.** Kinematics of our best-fitting spherical Jeans model of the mass distribution. The bottom panel compares to our data the model projected line-of-sight velocity dispersion of stars as a function of radius. The next panel upward shows the radial and tangential components $\sigma_r$ and $\sigma_t$, respectively, of the unprojected velocity dispersion. For readers who prefer to express the velocity anisotropy as $\beta \equiv 1 - \sigma_t^2/\sigma_r^2$, $\beta(r)$ is shown in the third panel. The top panel shows the circular-orbit rotation velocity of massless test particles embedded in the mass distribution. Results are shown for two dark matter (DM) halo models, the nonsingular isothermal and the Navarro et al. (1996, 1997) profile. The corresponding volume density profiles are shown in Figure 19. The stellar mass distribution is derived from the stellar light profile using $M/L_V \simeq 4$ derived from stellar population models (Maraston et al. 2003). Results on the stellar velocity anisotropy are robust to changes in the halo model: $\sigma_r > \sigma_t$ near the center, where $\sigma \sim 300$ km s$^{-1}$ is dominated by the galaxy; $\sigma_r < \sigma_t$ at intermediate radii, where $\sigma$ climbs to the cluster dispersion, and $\sigma_r > \sigma_t$ at large radii.

observed dispersion rises so rapidly that it is necessary to "boost" the line-of-sight component by increasing $\sigma_t$. Our conclusion that $\sigma_t > \sigma_r$ in the inner part of the cD halo of NGC 6166 is consistent with the suggestion that cD halo stars are the debris torn off of individual cluster galaxies by fast collisions (see, e.g., Puchwein et al. 2010).

In recent years, the growth of Sérsic $n > 4$ halos of giant, core-boxy-nonrotating elliptical galaxies (Kormendy 2009) has also been attributed to accumulated debris from minor mergers (e.g., Naab et al. 2009; Hopkins et al. 2010; Oser et al. 2010, 2012; Hilz et al. 2012, 2013). The relationship between these $n > 4$ halos—which manifestly belong to the galaxy—and the $n \simeq 8$ halo of NGC 6166—which manifestly belongs to the cluster—is a puzzle addressed in the following sections.
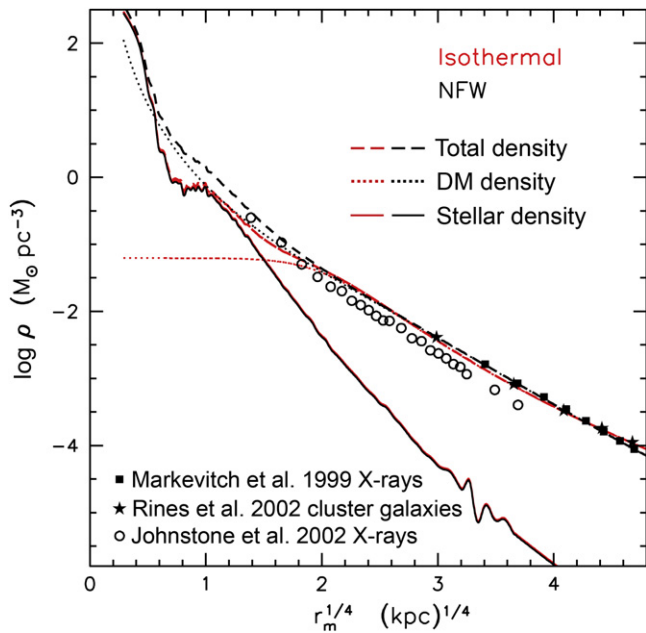
**Figure 19.** Volume mass densities in NGC 6166 given by the spherical Jeans models in Figure 18 for the isothermal and NFW dark matter halos. Here, $r_m$ is the geometric mean of major- and minor-axis radii. The DM scale radii are $r_s = 150$ kpc for NFW and $r_c = 20$ kpc for the isothermal sphere. The outer total density in our models is fitted to the filled stars, i.e., the mass density derived from the X-ray halo of the cluster Abell 2199 by Markevitch et al. (1999). The density similarly derived from X-ray emission by Johnstone et al. (2002) and the mass density as derived from the dynamics of cluster galaxies by Rines et al. (2002) are also shown for comparison.
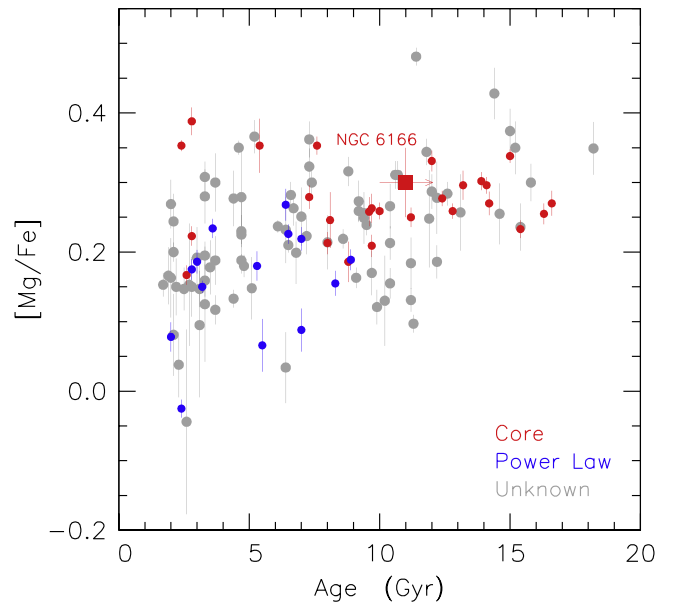


**Figure 20.** Correlation of [Mg/Fe] measure of $\alpha$ element (over)abundance with stellar population age showing core-boxy-nonrotating galaxies in red, coreless-disky-rotating galaxies in blue, and galaxies with unknown type in gray. The metallicity and age measurements are from Thomas et al. (2005); the galaxy classifications are from Lauer et al. (2007) or from KFCB, and this figure is from KFCB with NGC 6166 added.

At large $r$, the data hint that $\sigma_r > \sigma_t$. This as a preliminary result. If it is correct, it could be a sign that even at $\sim 100$ kpc, we reach radii where infall from the filaments of the cosmic web affect the velocity distribution (cf. Biviano et al. 2013; Wu et al. 2014).

The isothermal halo parameters derived here, $r_c = 20$ kpc and $\rho_0 = 6.2 \times 10^{-2}\ M_\odot\ \mathrm{pc}^{-3}$ for $M_B \simeq -23$, deviate from the DM parameter correlations found by Kormendy & Freeman (2015). The DM halo of NGC 6166 is more compact (e.g., higher in projected surface density) than expected from halos of late-type galaxies. However, it is consistent with scaling relations for cluster halos (Chan 2014), and its parameters agree with those derived for Abell 2199 by Chen et al. (2007).

## 6. HEAVY ELEMENT ABUNDANCES

Our high S/N spectra also allow us to probe stellar population diagnostics out into the part of the cD halo where the velocity dispersion is climbing to the cluster value. In Figure 20, we use the Lick Observatory spectral line indices (Faber et al. 1985; Gorgas et al. 1993; Worthey et al. 1994; Trager et al. 1998; Lee & Worthey 2005; Lee et al. 2009) to estimate Fe abundances and [Mg/Fe]—i.e., $\alpha$ element—over-abundances in the main body and cD halo of NGC 6166.

Overabundances with respect to solar values of $\alpha$ elements such as Mg imply short star formation time scales. Rapid enrichment of $\alpha$ elements follows starbursts when high-mass stars die as supernovae of Type II. Alpha elements then get diluted by Fe once lower-mass stars have time to die as white dwarfs and then blow up as supernovae of Type Ia. After that, [$\alpha$/Fe] can never be enhanced again. Therefore super-solar

[$\alpha$/Fe] abundances imply that almost all star formation was completed in $\lesssim 1$ Gyr (Worthey et al. 1992; Terndrup 1993; Matteucci 1994; Bender & Paquet 1995; Thomas et al. 1999, 2002, 2005). Small amounts of star formation seen in some BCGs and cDs (Oemler et al. 2009; Voit et al. 2015) cannot add up to a significant luminosity-weighed dilution of the [$\alpha$/Fe]-enhanced starlight.

KFCB show (Figure 20 here) that [$\alpha$/Fe] (over)abundance participates in the dichotomy (see Kormendy & Bender 1996; Kormendy 2009 for brief reviews) between giant, nonrotating, anisotropic ellipticals that have boxy isophotes and cuspy cores and lower-luminosity ellipticals that rotate enough to be more nearly isotropic and that have disky isophotes and (in general) central extra light components. They argue that rotating-coreless-disky ellipticals formed via at least one wet merger in which a starburst constructed the central extra component. And they argue that nonrotating-core-boxy ellipticals—which are embedded in large amounts of X-ray-emitting gas—formed most recently via dry major mergers (plus, we now believe, minor-merger addition of outer halos), protected from late star formation by their X-ray gas halos. Kormendy et al. (2009) found that [$\alpha$/Fe] is significantly more enhanced in nonrotating-core-boxy ellipticals than in rotating-coreless-disky ellipticals (cf. Thomas et al. 2005, 2010). Essentially all star formation was completed very early in these galaxies. NGC 6166 is a giant core elliptical (Figures 9–13, 15–17, 19) that participates in the profile-[Mg/Fe] dichotomy (Figure 20).

This machinery provides a partial test of our picture that cD halos consist of tidal debris torn from cluster galaxies. If [$\alpha$/Fe] is super-solar in the main body of NGC 6166 but near-solar in its cD halo and in smaller cluster galaxies, then this strongly supports the idea that cD halos consist of tidal debris. In contrast, if [$\alpha$/Fe] is super-solar in both the main body and the cD halo of NGC 6166, then this is consistent with our picture but does not prove it. Rather, that result is interesting because it

**Table 4**
Line Strength Measurements in NGC 6166

| Radius (arcsec) | Mg b (Å) | ⟨Fe⟩ (Å) | S/N (Å$^{-1}$) |
|---|---|---|---|
| 1.6 | 4.725 ± 0.098 | 2.772 ± 0.106 | 86 |
| 2.8 | 4.713 ± 0.085 | 2.641 ± 0.090 | 99 |
| 4.2 | 4.556 ± 0.101 | 2.668 ± 0.107 | 84 |
| 5.8 | 4.531 ± 0.105 | 2.522 ± 0.112 | 80 |
| 7.7 | 4.588 ± 0.119 | 2.525 ± 0.127 | 71 |
| 11.2 | 4.167 ± 0.097 | 2.261 ± 0.104 | 88 |
| 17.8 | 3.757 ± 0.127 | 2.245 ± 0.140 | 69 |
| 28.9 | 4.108 ± 0.184 | 1.944 ± 0.230 | 50 |
| 59.4 | 4.633 ± 0.480 | 2.725 ± 0.664 | 26 |

**Note.** Columns list the radius, the equivalent width of Mg b, the mean equivalent width of the Fe λ 5270 Å and 5335 Å lines, and the signal-to-noise ratio for the binned spectrum. Some of the binned spectra are shown in Figure 3.

suggests that star formation was switched off early in all galaxies that contribute to any part of NGC 6166. If so, then this result predicts that many (not necessarily all) smaller galaxies in the cluster are [α/Fe] enhanced, too. We do not have such data. But if spectroscopy of the smaller galaxies shows that they have solar [α/Fe] abundances whereas the cD halo has super-solar [α/Fe], then this argues *against* our picture and instead supports a picture in which all of the cD including its halo forms early via some special process. We carry out the first part of the test, measuring only NGC 6166.

Table 4 lists our line strength measurements in the central spectrum (*white line* in Figure 1) after binning it as in Figure 3 to provide the necessary high S/N (Column 4). A full description of the line strength measurement technique is given in Beuing et al. (2002). S/N estimation for the spectra and error calculation have been performed via Monte Carlo simulations as described in Bender et al. (1994).

Figure 21 shows our measurements in NGC 6166 of the Fe mean equivalent width versus that of Mg b. The iron lines used are Fe λ 5270 Å and 5335 Å. Colors encode radii whose corresponding velocity dispersions are given in the key. Thus, the red and orange points are dominated by light from the central galaxy, whereas the green point and especially the blue point increasingly measure stars in the cluster-σ cD halo.

Also shown are black points at specific metallicities and population ages (*lower key*) for three [α/Fe] abundance ratios. The points are connected by solid lines for ages of ∼10 Gyr and by dashed lines for ages of ∼3 Gyr. The models are from Thomas et al. (2003), Maraston et al. (2003), and Thomas & Maraston (2003).

Including $V - I$ color (Figure 9) and $H\beta$ information, we conclude that the central, $\sigma \leqslant 400$ km s$^{-1}$ parts of NGC 6166 are old ($\geqslant 11$ Gyr) and slightly more metal-rich than solar. They have [α/Fe] ≃ 0.3 ± 0.05. These observations are consistent with the E–E dichotomy (KFCB; Figure 20 here).

At radii $r \simeq 11''$–$18''$, where $\sigma$ begins to rise, the abundance is more nearly solar but [α/Fe] remains high.

In the inner cD halo, where rising $\sigma$ indicates that we see substantial (*green point*) and mostly (*blue point*) cluster halo ($\sigma \sim 800$ km s$^{-1}$) stars, the metallicity remains at least as high as at intermediate radii and [α/Fe] remains at $\gtrsim 0.3$. This is consistent with but does not prove that the cD halo consists of tidally liberated galaxy debris.
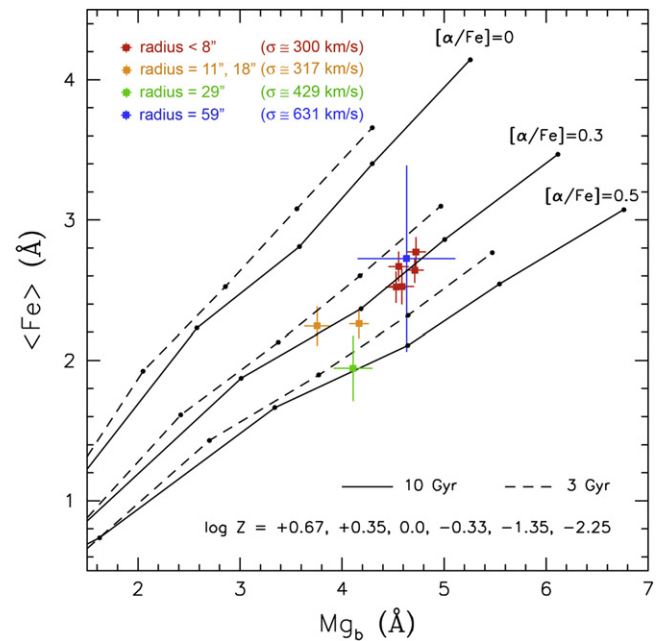


**Figure 21.** Correlation of ⟨Fe⟩ equivalent width with that of the Mg b lines along the central slit position of NGC 6166 as a function of radius. The measurements are on the Lick system. Model lines for various stellar population ages, metal abundances Z, and α element overabundances [α/Fe] are also shown (see the text for sources).

Similar tests have been carried out in normal ellipticals (e.g., Coccato et al. 2010). Greene et al. (2012, 2013) study 33 ellipticals with central $\sigma \geqslant 150$ km s$^{-1}$, not quite high enough to single out core galaxies. Quoting from the latter paper (Greene et al. 2013, page 1): "the typical star at $2r_e$ is old (∼10 Gyr), relatively metal-poor ([Fe/H] ≈ −0.5), and α-enhanced ([Mg/Fe] ≈ 0.3). Stars at large radii have different abundance ratio patterns from stars in the *center* of any present-day galaxy, but are similar to average Milky Way thick disk stars. Our observations are consistent with a picture in which the stellar outskirts are built up through minor mergers with disky galaxies whose star formation is truncated early ($z \approx 1.5$–$2$)."

## 7. EVOLUTIONARY HISTORY OF NGC 6166 AND ABELL 2199

If the cD halo of NGC 6166 had its star formation quenched in $\lesssim 1$ Gyr, then the environs of NGC 6166 have been special for a long time. This has implications for cD formation:

Kormendy (2015) reviews the substantial convergence by many lines of research on a consistent and plausible picture of what quenches star formation in general and especially in giant galaxies such as NGC 6166. The essential idea is often called "$M_{\rm crit}$ quenching:" a total galaxy or cluster mass $M \gtrsim M_{\rm crit} \sim 10^{12} M_\odot$ is required to hold gravitationally onto large amounts of hot, X-ray-emitting gas, and the hot gas quenches star formation. Essentially equivalent pictures have been reached (1) via theoretical studies of cosmological gas accretion onto large potential wells (Dekel & Birnboim 2006, 2008); (2) via semi-analytic modeling (Cattaneo et al. 2006, 2008, 2009); (3) via studies of galaxies in the high-redshift universe (e.g., Faber et al. 2007; Peng et al. 2010; Knobel et al. 2015); (4) via studies of physical differences between the two kinds of elliptical galaxies (KFCB; Kormendy & Bender

2012), and (5) via studies of AGN feedback in relation to the demographics of supermassive black holes and the properties of their host galaxies (Kormendy & Ho 2013). Note that the value of $M_{crit}$ is somewhat higher at higher $z$ because of higher cold gas fractions there (see the Dekel & Birnboim papers).

Peng et al. (2010) provide the clearest description: They distinguish mass-driven quenching from environmentally driven quenching and quenching related to bulge formation. Like Knobel et al. (2015), we suggest that mass-driven and environmentally driven quenching are fundamentally the same process; in mass-driven quenching, the quenched galaxy owns its own hot gas, whereas in environmentally driven quenching of satellite galaxies, the gas that does the work belongs to the parent giant galaxy or cluster. Both processes together are equivalent to the "maintenance-mode AGN feedback" discussed in Kormendy & Ho (2013). Again, the quenching is done by the hot gas, and the process that keeps it hot (AGN feedback is one possibility) is somewhat secondary. Quenching by hot gas is the essential process that is relevant here. (Peng's "quenching associated with bulge formation" is equivelent to Kormendy & Ho's "quasar-mode feedback.")

The X-ray halo needed for $M_{crit}$ quenching is present in Abell 2199 (e.g., Markevitch et al. 1999; Johnstone et al. 2002; Kawaharada et al. 2010). However, the implications of our results are broader than this:

In general, we expect that a cluster grows as galaxies and galaxy groupings fall into it that are sufficiently sub-$M_{crit}$ to have had prolonged star formation histories. As they and their stars get added to NGC 6166, it is natural to expect that the resulting halo would not be as $\alpha$ element enhanced as the main body of the galaxy. Simulations suggest that cD halo stars are somewhat older than typical stars in the galaxies that contribute to the halo (Murante et al. 2004; Puchwein et al. 2010). Also, simulations by Murante et al. (2007) suggest that the inner parts of cD halos—this certainly includes the parts of NGC 6166 that we have measured—"come from the [merger] family tree of the [parent galaxy];" that is, from galaxies that share the immediate history of the central galaxy. And simulators agree that the halo tends to be contributed by the most massive cluster galaxies; their star formation was presumably quenched early. Still, if even the debris halo of NGC 6166 is $\alpha$ element enhanced, then this suggests that the environs of the galaxy—including that of the progenitors that contributed to its cD halo—constituted a deep enough gravitational potential well to allow star formation to be quenched rapidly. And this suggests a solution to the following puzzle:

Why does NGC 6166 have such a high-surface-brightness halo of intracluster stars when apparently richer and denser clusters such as Coma have weaker cD characteristics? Note that the velocity dispersion has already risen significantly in NGC 6166 at $r \sim 30''$ (Figures 4 and 5), where the surface brightness is $\sim 22.5$ $V$ mag arcsec$^{-2}$ (Table 3). Evidently the processes that freed the intracluster stars happened less strongly or for a shorter time in Coma than in Abell 2199. Why?

Coma may have formed relatively recently—is, in fact, still forming now, with the imminent accretion of the NGC 4839 grouping (see Section 2.1.1). In contrast, Abell 2199 looks less dense than Coma does now, but the central few hundred kpc volume evidently has been a massive enough environment to allow the early quenching of star formation. It may also have been dense enough to allow cD halo formation processes to operate efficiently for an unusually long time.

A more speculative remark follows from the large core radius of NGC 6166 (Figure 13). There is a tight correlation between the light and mass "deficit" that defines the core phenomenon and the measured mass $M_\bullet$ of supermassive black holes (Kormendy & Bender 2009). The canonical interpretation is that cores are created when supermassive black hole binaries produced in major, dry mergers fling stars away from the center as they decay toward an eventual merger (e.g., Ebisuzaki et al. 1991; Faber et al. 1997; Milosavljević & Merritt 2001; Milosavljević et al. 2002; Merritt 2006). If the $M_\bullet$–core correlation is valid for NGC 6166, then the core light deficit $M_{V,def} \simeq -19.67$ corresponds to a BH mass of $M_\bullet = 4.1^{+1.4}_{-1.1} \times 10^9 \, M_\odot$. The core radius is unusually large, but the core surface brightness is unusually small. So the light deficit and $M_\bullet$ are almost the same as those of M87. Still, Abell 2199 is one of the most plausible environments in which episodic AGN feedback could help to keep its hot gas hot (Fabian 2012). And the early quenching of star formation together with the long history of cluster dynamical evolution may be connected with the unusual properties (large radius but low surface brightness) of the core of NGC 6166.

## 8. IMPLICATIONS FOR cD FORMATION MECHANISMS

This observational paper does not fully review the large literature on possible formation mechanisms for cD galaxies. We restrict ourselves to the most basic conclusions from our new results and concentrate on formation of the cD halo. Suggested mechanisms are divided into three categories:

### 8.1. Star Formation in Cooling Flows in X-Ray Gas

Are cD halos made of stars that rain out of cooling flows in hot gas (see Fabian et al. 1991; Fabian 1994 for reviews)? This idea was entertained in the heyday of the cooling-flow problem, when we observed large amounts of X-ray-emitting, hot gas in clusters but could not measure temperature profiles. Absent heating processes, hot-gas cooling times near the centers of many clusters and individual galaxies are short. In clusters, $10^2$–$10^3 \, M_\odot$ yr$^{-1}$ of baryons should rain out of the hot gas, presumably by star formation. To escape detection, the initial mass function would have to be truncated above $\sim 1 \, M_\odot$ (Fabian et al. 1991). We have never directly observed such star formation in any environment (Bastian et al. 2010).

This possibility is now regarded as a non-starter. The main reason is that we now can measure gas temperature profiles, and we find that temperatures decrease only modestly to a floor at $kT \sim 1$ keV. In particular, we do not see the strong emission lines from Fe XVII that would be our signal that gas has cooled below 0.7 keV (see Fabian 2012 for review). So the cooling flow problem has morphed into a different question: what keeps the gas hot? At least three heating processes are hard to avoid. Most popular is heating by AGN feedback (Fabian 2012; Kormendy & Ho 2013; Heckman & Best 2014 provide reviews). Also, gas from the cosmological web that falls into objects with masses $M > M_{crit} \sim 10^{12} \, M_\odot$ accelerates so much that a shock forms where it impacts the static intergalactic or intracluster medium; this heats the hot gas from the outside inward (Birnboim & Dekel 2003; Kereš et al. 2005; Dekel & Birnboim 2006, 2008). This is an aspect of $M_{crit}$ quenching of star formation. Finally, dying stars eject large amounts of mass into the intracluster medium at the kinetic temperatures of stars

in galaxies and galaxies in clusters (e.g., Ostriker 2006). All three mechanisms are likely to be important. In this picture, episodic cooling fuels the AGN and switches it on long enough to allow it to keep the center of the hot gas hot (Fabian 2012). Small amounts of star formation may be connected with these events, and small amounts of star formation are seen in brightest cluster galaxies (e.g., Liu et al. 2012). But no compelling argument suggests that large amounts of star formation occur in clusters at radii where we see cD halos. Also, our observation that the cD halo of NGC 6166 is $\alpha$ element enriched precludes the idea that prolonged, in situ star formation made a significant fraction of the light that we see in the halo.

### 8.2. Processes Intrinsic to the Origin of the Central Galaxy

Do cD halos originate as an integral part of the formation of the central galaxy? For example, could a specialized history of galaxy mergers make both the central and halo parts of a cD galaxy together?

Our phrasing is somewhat different from the question that dominated work on brightest cluster galaxies (BCGs) in the 1970s–1990s (see Tremaine 1990 for a review). Then, the emphasis was on observational hints that BCGs in general (i.e., including but not limited to cDs) are inconsistent with statistical expectations based on the luminosity functions $\phi(L)$ of fainter galaxies in the cluster. If $\phi \propto L^\alpha \exp(-L/L^*)$ with characteristic luminosity $L^*$ (Schechter 1976), then BCGs with $L \sim 10\,L^*$ are statistically too bright to be drawn from the populations of other galaxies in the clusters (see Figure 1 in Binggeli 1987 for an evocative illustration). In many papers, cDs and non-cD BCGs were discussed together. Given the observation that cD halos are approximately as bright as or brighter than the central parts of the galaxies (e.g., Seigar et al. 2007), this essentially ensures that BCGs as a class will look especially luminous (Tremaine & Richstone 1977).

As some authors have done since the beginning of this subject, we differentiate between the main bodies of cDs and their halos. In NGC 6166, we separate them operationally as having $\sigma \simeq 300$ and $\sigma \sim 832\,\mathrm{km\,s^{-1}}$, respectively. How the main bodies of BCGs form and how cD halos form may be separate questions.

When their halos are inventoried separately, it is much less obvious that the main bodies of cDs are unusual enough to imply formation physics that is different from that of other cluster galaxies. The new observations in this paper do not speak strongly to this issue, and we do not discuss it in detail. Ways in which the main body of NGC 6166 is *not* unusual are the subject of Sections 3.2–3.5. Except for its unusually large and low-surface-brightness core (discussed in the previous section), the main body of NGC 6166 is rather like M87 (a marginal cD) but also like the other giant-core-boxy ellipticals in the Virgo cluster. Quantitative differences (Section 3.6) are mainly due to the cD halo of NGC 6166. However, we note here one additional observation that *does* imply something special about cD-like galaxies:

Prototypical of a compelling but mysterious phenomenon, M87 has an unusually large number of globular clusters for its galaxy luminosity. Harris & van den Bergh (1981) introduced the specific globular cluster frequency $S_N$ as the number of globulars per unit absolute magnitude $M_V = -15$ of galaxy luminosity. Measurement of $S_N$ is tricky for many reasons (e.g., galaxy distances are uncomfortably large, so we see less deeply into cluster luminosity functions than we would like), but the

conclusion that $S_N \sim 10$ is factors of several larger for M87 and for some other BCGs (e.g., NGC 1399: Hanes & Harris 1986; Harris & Hanes 1987; NGC 3311: Harris 1986; see Harris et al. 2013 for the most recent summary) has withstood the test of time. The number of globular clusters in NGC 6166 is $N_{GC} = 17{,}000 \pm 4000$ (Harris et al. 2013). With respect to the absolute magnitude of the main E-like part of NGC 6166, this implies that $S_N \simeq 12$. If instead we normalize $N_{GC}$ by the total luminosity including the cD halo, then $S_N \sim 4$. This is still slightly higher than the canonical number of $1 \pm 1$ (full scatter for almost all objects) for $L^*$ ellipticals (Harris et al. 2013, Figure 10). In this sense, NGC 6166 is consistent with the behavior of other, similar-luminosity systems (see the Harris paper). As discussed, for example, in Burkert & Tremaine (2010), this is one indication that the early evolution of the objects that later assembled into these BCGs (some of which are clearly cDs and others of which are just giant ellipticals) was already special. This theme of an early, special environment in which NGC 6166 and its cD halo formed was discussed here in Section 7.

### 8.3. cD Halo Formation by Stellar-dynamical Processes Inherent to Clusters

Our observations are most consistent with the now favored picture that cD halos are constructed by stellar-dynamical processes that are inherent to cluster evolution. The main body forms by the usual hierarchical clustering and galaxy merging, especially in smaller group precursors to present-day, rich clusters. In the process, violent relaxation splashes some stars to large radii. But the cD halo is added as a result of cluster-related processes such as the stripping of stars off of member galaxies by dynamical harassment and the cannibalism and destruction of dwarf galaxies in minor mergers. This picture was originated by Gallagher & Ostriker (1972) and by Richstone (1975, 1976) and has now been greatly elaborated in many papers, both observational (see the earlier papers on cluster background light and, e.g., Bernstein et al. 1995; Gonzalez et al. 2005; Arnaboldi et al. 2012; Montes & Trujillo 2014) and theoretical (e.g., Dubinski 1998; Murante et al. 2004, 2007; De Lucia & Blaizot 2007; Puchwein et al. 2010; and Cui et al. 2014).

### 8.4. Blurring the Distinction Between cD Galaxies and Elliptical Galaxies with Cores

Our observations (1) that the cD halo of NGC 6166 is more nearly at rest in Abell 2199 than is its central galaxy and (2) that this halo has the same velocity dispersion as the cluster galaxies support the idea that it consists of stars that were liberated from cluster members. The high velocity dispersion implies that the cD halo is controlled by cluster gravity. It is only by convention—and not because this is physically meaningful—that we call it the halo of NGC 6166.

On the other hand, the outer parts of NGC 6166 and the ICL merge seamlessly such that the brightness profile outside the central core is well described by a single Sérsic function with index $n \simeq 8$. In this sense, NGC 6166 qualitatively resembles other core-boxy-nonrotating elliptical galaxies such as those studied in KFCB and emphasized in the SAURON/Atlas[3D] series of papers (see M. Cappellari 2015, in preparation for a review). The Sérsic $n > 4$ halos of core-boxy-nonrotating ellipticals that are not BCGs manifestly belong to the galaxy:

their velocity dispersions generally decrease monotonically outward.

This blurs the distinction between cDs and giant elliptical galaxies. Perhaps they are more similar than we thought. The central puzzle about both kinds of galaxies is why $n > 4$. In contrast, many numerical simulations of major mergers of two similar galaxies robustly show that the scrambled-up remnants of the stars that were already present before the mergers have Sérsic profiles with $n \sim 3 \pm 1$ (e.g., van Albada 1982; Mihos & Hernquist 1994; Springel & Hernquist 2005; Naab & Trujillo 2006; Hopkins et al. 2009a, 2009b). These are precisely the Sérsic indices observed for coreless-disky-rotating ellipticals, which are thought to be formed in wet mergers during which starbursts grew the central extra light components (see Kormendy 1999 and KFCB for observations and review and Hopkins et al. 2009a for the most detailed simulations).

Maybe the main difference between cDs and core-boxy-nonrotating (but not cD) ellipticals is the degree to which clusters are dynamically old enough to have liberated enough stars from individual galaxies to make a detectable intracluster population. It may also matter whether the large-$n$ halos formed in subgroups such that the central galaxy controls their dynamics or conversely in high-$\sigma$, rich clusters at radii controlled by the cluster rather than the central galaxy. An important goal of future work is to explore the reasons why cD galaxies and core-boxy-nonrotating ellipticals look so similar when their halo velocity dispersions point to significant differences in formation histories.

## REFERENCES

Andrade-Santos, F., Nulsen, P. E. J., Kraft, R. P., et al. 2013, ApJ, 766, 107
Arnaboldi, M. 2011, Paper presented at the ESO Workshop on Fornax, Virgo, Coma et al.: Stellar Systems in High Density Environments, ed. M. Arnaboldi http://www.eso.org/sci/meetings/2011/fornax_virgo2011/talks_pdf/Arnaboldi_Magda.pdf
Arnaboldi, M., Aguerri, J. A. L., Napolitano, N. R., et al. 2002, AJ, 123, 760
Arnaboldi, M., Freeman, K. C., Mendez, R. H., et al. 1996, ApJ, 472, 145
Arnaboldi, M., & Gerhard, O. 2010, HiA, 15, 97
Arnaboldi, M., Gerhard, O., Aguerri, J. A. L., et al. 2004, ApJL, 614, L33
Arnaboldi, M., Ventimiglia, G., Iodice, E., Gerhard, O., & Coccato, L. 2012, A&A, 545, A37
Baggett, W. E., Baggett, S. M., & Anderson, K. S. J. 1998, AJ, 116, 1626
Bastian, N., Covey, K. R., & Meyer, M. R. 2010, ARA&A, 48, 339
Beers, T. C., & Geller, M. J. 1983, ApJ, 274, 491
Bender, R. 1987, MitAG, 226
Bender, R. 1988, A&A, 193, L7
Bender, R. 1990, A&A, 229, 441
Bender, R., Burstein, D., & Faber, S. M. 1992, ApJ, 399, 462
Bender, R., Burstein, D., & Faber, S. M. 1993, ApJ, 411, 153
Bender, R., Döbereiner, S., & Möllenhoff, C. 1987, A&A, 177, L53
Bender, R., Döbereiner, S., & Möllenhoff, C. 1988, A&AS, 74, 385
Bender, R., & Möllenhoff, C. 1987, A&A, 177, 71

Bender, R., & Paquet, A. 1995, in IAU Symp. 164, Stellar Populations, ed. P. C. van der Kruit & G. Gilmore (Dordrecht: Kluwer), 259
Bender, R., Saglia, R. P., & Gerhard, O. E. 1994, MNRAS, 269, 785
Bender, R., Surma, P., Döbereiner, S., Möllenhoff, C., & Madejsky, R. 1989, A&A, 217, 35
Bernstein, G. M., Nichol, R. C., Tyson, J. A., Ulmer, M. P., & Wittman, D. 1995, AJ, 110, 1507
Beuing, J., Bender, R., Mendes de Oliveira, C., Thomas, D., & Maraston, C. 2002, A&A, 395, 431
Binggeli, B. 1987, in Nearly Normal Galaxies: From the Planck Time to the Present, ed. S. M. Faber (New York: Springer), 195
Birnboim, Y., & Dekel, A. 2003, MNRAS, 345, 349
Biviano, A., Rosati, P., Balestra, I., et al. 2013, A&A, 558, A1
Briel, U. G., Henry, J. P., Lumb, D. H., et al. 2001, A&A, 365, L60
Buitrago, F., Trujillo, I., Conselice, C. J., et al. 2008, ApJL, 687, L61
Burbidge, E. M. 1962, ApJ, 136, 1134
Burkert, A., & Tremaine, S. 2010, ApJ, 720, 516
Byun, Y.-I., Grillmair, C. J., Faber, S. M., et al. 1996, AJ, 111, 1889
Cappellari, M. 2002, MNRAS, 333, 400
Carter, D., Bridges, T. J., & Hau, G. K. T. 1999, MNRAS, 307, 131
Carter, D., Efstathiou, G., Ellis, R. S., Inglis, I., & Godwin, J. 1981, MNRAS, 195, 15P
Carter, D., Inglis, I., Ellis, R. S., Efstathiou, G., & Godwin, J. G. 1985, MNRAS, 212, 471
Castro-Rodriguéz, N., Arnaboldi, M., Aguerri, J. A. L., et al. 2009, A&A, 507, 621
Cattaneo, A., Dekel, A., Devriendt, J., Guiderdoni, B., & Blaizot, J. 2006, MNRAS, 370, 1651
Cattaneo, A., Dekel, A., Faber, S. M., & Guiderdoni, B. 2008, MNRAS, 389, 567
Cattaneo, A., Faber, S. M., Binney, J., et al. 2009, Natur, 460, 213
Chan, M. H. 2014, MNRAS, 442, L14
Chen, Y., Reiprich, T. H., Böhringer, H., Ikebe, Y., & Zhang, Y.-Y. 2007, A&A, 466, 805
Chiboucas, K., Karachentsev, I. D., & Tully, R. B. 2009, AJ, 137, 3009
Churazov, E., Forman, W., Vikhlinin, A., et al. 2008, MNRAS, 388, 1062
Coccato, L., Gerhard, O., & Arnaboldi, M. 2010, MNRAS, 407, L26
Côté, P., McLaughlin, D. E., Hanes, D. A., et al. 2001, ApJ, 559, 828
Coziol, R., Andernach, H., Caretta, C. A., Alamo-Martínez, K. A., & Tago, E. 2009, AJ, 137, 4795
Cui, W., Murante, G., Monaco, P., et al. 2014, MNRAS, 437, 816
Dekel, A., & Birnboim, Y. 2006, MNRAS, 368, 2
Dekel, A., & Birnboim, Y. 2008, MNRAS, 383, 119
De Lucia, G., & Blaizot, J. 2007, MNRAS, 375, 2
Djorgovski, S. 1992, in Morphological and Physical Classification of Galaxies, ed. G. Longo, M. Capaccioli, & G. Busarello (Dordrecht: Kluwer), 337
Djorgovski, S., & Davis, M. 1987, ApJ, 313, 59
Djorgovski, S., de Carvalho, R., & Han, M.-S. 1988, in The Extragalactic Distance Scale, ed. S. van den Bergh, & C. J. Pritchet (San Francisco, CA: ASP), 329
Doherty, M., Arnaboldi, M., Das, P., et al. 2009, A&A, 502, 771
Donzelli, C. J., Muriel, H., & Madrid, J. P. 2011, ApJS, 195, 15
Dressler, A. 1979, ApJ, 231, 659
Dressler, A., Lynden-Bell, D., Burstein, D., et al. 1987, ApJ, 313, 42
Dubinski, J. 1998, ApJ, 502, 141
Ebisuzaki, T., Makino, J., & Okamura, S. K. 1991, Natur, 354, 212
Emsellem, E., Monnet, G., & Bacon, R. 1994, A&A, 285, 723
Faber, S. M., Dressler, A., Davies, R. L., et al. 1987, in Nearly Normal Galaxies: From the Planck Time to the Present, ed. S. M. Faber (New York: Springer), 175
Faber, S. M., Friel, E. D., Burstein, D., & Gaskell, C. M. 1985, ApJS, 57, 711
Faber, S. M., Tremaine, S., Ajhar, E. A., et al. 1997, AJ, 114, 1771
Faber, S. M., Willmer, C. N. A., Wolf, C., et al. 2007, ApJ, 665, 265
Fabian, A. C. 1994, ARA&A, 32, 277
Fabian, A. C. 2012, ARA&A, 50, 455
Fabian, A. C., Nulsen, P. E. J., & Canizares, C. R. 1991, A&AR, 2, 191
Ferrarese, L., Côté, P., Jordán, A., et al. 2006, ApJS, 164, 334
Fisher, D. B., & Drory, N. 2008, AJ, 136, 773
Fisher, D., Illingworth, G., & Franx, M. 1995, ApJ, 438, 539
Foster, C., Spitler, L. R., Romanowsky, A. J., et al. 2011, MNRAS, 415, 3393
Gallagher, J. S., & Ostriker, J. P. 1972, AJ, 77, 288
Gavazzi, G., Donati, A., Cucciati, O., et al. 2005, A&A, 430, 411
Gavazzi, G., Franzetti, P., Scodeggio, M., Boselli, A., & Pierini, D. 2000, A&A, 361, 863
Gebhardt, K., & Thomas, J. 2009, ApJ, 700, 1690
Gebhardt, K., Richstone, D., Ajhar, E. A., et al. 1996, AJ, 112, 105

Gerhard, O., Arnaboldi, M., Freeman, K. C., et al. 2007, A&A, 468, 815
Gonzalez, A. H., Zabludoff, A. I., & Zaritsky, D. 2005, ApJ, 218, 195
Gorgas, J., Faber, S. M., Burstein, D., et al. 1993, ApJS, 86, 153
Greene, J. E., Murphy, J. D., Comerford, J. M., Gebhardt, K., & Adams, J. J. 2012, ApJ, 750, 32
Greene, J. E., Murphy, J. D., Graves, G. J., et al. 2013, ApJ, 776, 64
Hanes, D. A., & Harris, W. E. 1986, ApJ, 309, 564
Harris, W. E. 1986, AJ, 91, 822
Harris, W. E., & Hanes, D. A. 1987, AJ, 93, 1368
Harris, W. E., Harris, G. L. H., & Alessi, M. 2013, ApJ, 772, 82
Harris, W. E., & van den Bergh, S. 1981, AJ, 86, 1627
Heckman, T. M., & Best, P. N. 2014, ARA&A, 52, 589
Hill, G. J., Nicklas, H. E., MacQueen, P. J., et al. 1998, Proc. SPIE, 3355, 375
Hilz, M., Naab, T., & Ostriker, J. P. 2013, MNRAS, 429, 2924
Hilz, M., Naab, T., Ostriker, J. P., et al. 2012, MNRAS, 425, 3119
Hopkins, P. F., Bundy, K., Hernquist, L., Wuyts, S., & Cox, T. J. 2010, MNRAS, 401, 1099
Hopkins, P. F., Cox, T. J., Dutta, S. N., et al. 2009a, ApJS, 181, 135
Hopkins, P. F., Lauer, T. R., Cox, T. J., Hernquist, L., & Kormendy, J. 2009b, ApJS, 181, 486
Huang, S., Ho, L. C., Peng, C. Y., Zhao-Yu, L., & Barth, A. J. 2013a, ApJ, 766, 47
Huang, S., Ho, L. C., Peng, C. Y., Zhao-Yu, L., & Barth, A. J. 2013b, ApJL, 768, L28
Hubble, E. 1936, The Realm of the Nebulae (New Haven: Yale Univ. Press)
Johansson, P. H., Naab, T., & Ostriker, J. P. 2012, ApJ, 754, 115
Johnstone, R. M., Allen, S. W., Fabian, A. C., & Sanders, J. S. 2002, MNRAS, 336, 299
Kawaharada, M., Makishima, K., Kitaguchi, T., et al. 2010, PASJ, 62, 115
Kelson, D. D., Zabludoff, A. I., Williams, K. A., et al. 2002, ApJ, 576, 720
Kereš, D., Katz, N., Weinberg, D. H., & Davé, R. 2005, MNRAS, 363, 2
Knobel, C., Lilly, S. J., Woo, J., & Kovač, K. 2015, ApJ, 800, 24
Komatsu, E., Dunkley, J., Nolta, M. R., et al. 2009, ApJS, 180, 330
Kormendy, J. 1999, in ASP Conf. Ser. 182, Galaxy Dynamics: A Rutgers Symposium, ed. D. Merritt, J. A. Sellwood, & M. Valluri (San Francisco, CA: ASP), 124
Kormendy, J. 2009, in ASP Conf. Ser. 419, Galaxy Evolution: Emerging Insights and Future Challenges, ed. S. Jogee et al. (San Francisco, CA: ASP), 87
Kormendy, J. 2015, in Galactic Bulges, ed. E. Laurikainen, R. F. Peletier, & D. A. Gadotti (New York: Springer), in press (arXiv:1504.03330)
Kormendy, J., & Bender, R. 1996, ApJL, 464, L119
Kormendy, J., & Bender, R. 2009, ApJL, 691, L142
Kormendy, J., & Bender, R. 2012, ApJS, 198, 2
Kormendy, J., & Djorgovski, S. 1989, ARA&A, 27, 235
Kormendy, J., Dressler, A., Byun, Y.-I., et al. 1994, in ESO/OHP Workshop on Dwarf Galaxies, ed. G. Meylan & P. Prugniel (Garching: ESO), 147
Kormendy, J., & Freeman, K. C. 2015, ApJ, submitted (arXiv:1411.2170)
Kormendy, J., Fisher, D. B., Cornell, M. E., & Bender, R. 2009, ApJS, 182, 216 (KFCB)
Kormendy, J., & Ho, L. C. 2013, ARA&A, 51, 511
Kosyra, R., Gössl, C., Hopp, U., et al. 2014, ExA, 38, 213
Kronawitter, A., Saglia, R. P., Gerhard, O., & Bender, R. 2000, A&AS, 144, 53
Kroupa, P. 2001, MNRAS, 322, 231
Lachièze-Rey, M., Vigroux, L., & Souviron, J. 1985, A&A, 150, 62
Lauer, T. R. 1985, ApJS, 57, 473
Lauer, T. R. 1986, ApJ, 311, 34
Lauer, T. R., Ajhar, E. A., Byun, Y.-I., et al. 1995, AJ, 110, 2622
Lauer, T. R., Gebhardt, K., Faber, S. M., et al. 2007, ApJ, 664, 226
Lauer, T. R., Postman, M., Strauss, M. A., Graves, G. J., & Chisari, N. E. 2014, ApJ, 797, 82
Lee, H.-C., & Worthey, G. 2005, ApJS, 160, 176
Lee, H.-C., Worthey, G., Dotter, A., et al. 2009, ApJ, 694, 902
Liu, F. S., Mao, S., & Meng, X. M. 2012, MNRAS, 423, 422
Loubser, S. I., Sansom, A. E., Sánchez-Blázquez, P., Soechting, I. K., & Bromage, G. E. 2008, MNRAS, 391, 1009
Lucy, L. B. 1974, AJ, 79, 745
Maraston, C., Greggio, L., Renzini, A., et al. 2003, A&A, 400, 823
Markevitch, M., Vikhlinin, A., Forman, W. R., & Sarazin, C. L. 1999, ApJ, 527, 545
Martin, N. F., de Jong, J. T. A., & Rix, H.-W. 2008, ApJ, 684, 1075
Mateo, M. 1998, ARA&A, 36, 435
Matteucci, F. 1994, A&A, 288, 57
Matthews, T. A., Morgan, W. W., & Schmidt, M. 1964, ApJ, 140, 35
McConnachie, A. W., & Irwin, M. J. 2006, MNRAS, 365, 1263

Merritt, D. 1983, ApJ, 264, 24
Merritt, D. 2006, ApJ, 648, 976
Mihos, J. C. 2011, Paper presented at the ESO Workshop on Fornax, Virgo, Coma et al.: Stellar Systems in High Density Environments, ed. M. Arnaboldi http://www.eso.org/sci/meetings/2011/fornax_virgo2011/talks_pdf/Mihos_Chris.pdf
Mihos, J. C., Harding, P., Feldmeier, J., & Morrison, H. 2005, ApJL, 631, L41
Mihos, J. C., & Hernquist, L. 1994, ApJL, 437, L47
Mihos, J. C., Janowiecki, S., Feldmeier, J. J., Harding, P., & Morrison, H. 2009, ApJ, 698, 1879
Milosavljević, M., & Merritt, D. 2001, ApJ, 563, 34
Milosavljević, M., Merritt, D., Rest, A., & van den Bosch, F. C. 2002, MNRAS, 331, L51
Minkowski, R. 1961, AJ, 66, 558
Montes, M., & Trujillo, I. 2014, ApJ, 794, 137
Morgan, W. W. 1958, PASP, 70, 364
Morgan, W. W., & Lesh, J. R. 1965, ApJ, 142, 1364
Murante, G., Arnaboldi, M., Gerhard, O., et al. 2004, ApJL, 607, L83
Murante, G., Giovalli, M., Gerhard, O., et al. 2007, MNRAS, 377, 2
Murphy, J. D., Gebhardt, K., & Adams, J. J. 2011, ApJ, 729, 129
Murphy, J. D., Gebhardt, K., & Cradit, M. 2014, ApJ, 785, 143
Naab, T., Johansson, P. H., & Ostriker, J. P. 2009, ApJL, 699, L178
Naab, T., & Trujillo, I. 2006, MNRAS, 369, 625
Navarro, J. F., Frenk, C. S., & White, S. D. M. 1996, ApJ, 462, 563
Navarro, J. F., Frenk, C. S., & White, S. D. M. 1997, ApJ, 490, 493
Neumann, D. M., Arnaud, M., Gaustad, R., et al. 2001, A&A, 365, L74
Neumann, D. M., Lumb, D. H., Pratt, G. W., & Briel, U. G. 2003, A&A, 400, 411
Nowak, N., Saglia, R. P., Thomas, J., et al. 2008, MNRAS, 391, 1629
Oegerle, W. R., & Hill, J. M. 2001, AJ, 122, 2858
Oemler, A. 1976, ApJ, 209, 693
Oemler, A., Dressler, A., Kelson, D., et al. 2009, AJ, 693, 152
Oser, L., Naab, T., Ostriker, J. P., & Johansson, P. H. 2012, ApJ, 744, 63
Oser, L., Ostriker, J. P., Naab, T., Johansson, P. H., & Burkert, A. 2010, ApJ, 725, 2312
Ostriker, J. P. 2006, Paper Presented at the Thinkshop on The Role of Black Holes in Galaxy Formation and Evolution (Summarized in Cattaneo et al. 2009)
Ostriker, J. P., & Tremaine, S. D. 1975, ApJL, 202, L113
Papovich, C., Bassett, R., Lotz, J. M., et al. 2012, ApJ, 750, 93
Peng, Y.-J., Lilly, S. J., Kovač, K., et al. 2010, ApJ, 721, 193
Pimbblet, K. A., Roseboom, I. G., & Doyle, M. T. 2006, MNRAS, 368, 651
Proctor, R. N., Forbes, D. A., Romanowsky, A. J., et al. 2009, MNRAS, 398, 91
Puchwein, E., Springel, V., Sijacki, D., & Dolag, K. 2010, MNRAS, 406, 936
Quintana, H., & Lawrie, D. G. 1982, AJ, 87, 1
Raskutti, S., Greene, J. E., & Murphy, J. D. 2014, ApJ, 786, 23
Richardson, W. H. 1972, JOSA, 62, 52
Richstone, D. O. 1975, ApJ, 200, 535
Richstone, D. O. 1976, ApJ, 204, 642
Richstone, D. O., & Malumuth, E. M. 1983, ApJ, 268, 30
Rines, K., Geller, M. J., Diaferio, A., et al. 2002, AJ, 124, 1266
Sandage, A. 1961, The Hubble Atlas of Galaxies (Washington: Carnegie Institution of Washington)
Savage, B. D., & Mathis, J. S. 1979, ARA&A, 17, 73
Schechter, P. 1976, ApJ, 203, 297

Schlegel, D. J., Finkbeiner, D. P., & Davis, M. 1998, ApJ, 500, 525
Schombert, J. M. 1986, ApJS, 60, 603
Schombert, J. M. 1987, ApJS, 64, 643
Schombert, J. M. 1988, ApJ, 328, 475
Schwarzschild, M. 1979, ApJ, 232, 236
Schwarzschild, M. 1982, ApJ, 263, 599
Seigar, M. S., Graham, A. W., & Jerjen, H. 2007, MNRAS, 378, 1575
Sembach, K. R., & Tonry, J. L. 1996, AJ, 112, 797
Sérsic, J. L. 1968, Atlas de Galaxias Australes, (Córdoba: Observatório Astronómico, Univ. de Córdoba)
Simionescu, A., Werner, N., Urban, O., et al. 2013, ApJ, 775, 4
Skrutskie, M. F., Cutri, R. M., & Stiening, R. 2006, AJ, 131, 1163
Springel, V., & Hernquist, L. 2005, ApJL, 622, L9
Stover, R. J. 1988, in Instrumentation for Ground-Based Optical Astronomy: Present and Future, ed. L. B. Robinson (New York: Springer), 443
Szomoru, D., Franx, M., & van Dokkum, P. G. 2012, ApJ, 749, 121
Terndrup, D. M. 1993, in The Minnesota Lectures on the Structure and Dynamics of the Milky Way, ed. R. M. Humphreys (San Francisco, CA: ASP), 9
Thomas, D., Greggio, L., & Bender, R. 1999, MNRAS, 302, 537
Thomas, D., & Maraston, C. 2003, A&A, 401, 429
Thomas, D., Maraston, C., & Bender, R. 2002, Ap&SS, 281, 371
Thomas, D., Maraston, C., & Bender, R. 2003, MNRAS, 339, 897
Thomas, D., Maraston, C., Bender, R., & Mendez de Oliveira, C. 2005, ApJ, 621, 673
Thomas, D., Maraston, C., Schawinski, K., Sarzi, M., & Silk, J. 2010, MNRAS, 404, 1775
Tonry, J. L. 1984, ApJ, 279, 13
Tonry, J. L. 1985, AJ, 90, 2431
Trager, S. C., Worthey, G., Faber, S. M., Burstein, D., & González, J. J. 1998, ApJS, 116, 1
Tremaine, S. 1990, in Dynamics and Interactions of Galaxies, ed. R. Wielen (Berlin: Springer), 394
Tremaine, S., & Richstone, D. O. 1977, ApJ, 212, 311
van Albada, T. S. 1982, MNRAS, 201, 939
van Dokkum, P. G., Whitaker, K. E., Brammer, G., et al. 2010, ApJ, 709, 1018
Ventimiglia, G., Gerhard, O., Arnaboldi, M., & Coccato, L. 2010, A&A, 520, L9
Voit, G. M., Donahue, M., Bryan, G. L., & McDonald, M. 2015, Natur, 519, 203
Weijmans, A.-M., Cappellari., M., Bacon, R., et al. 2009, MNRAS, 398, 561
White, S. D. M. 1976, MNRAS, 174, 19
White, S. D. M., Briel, U. G., & Henry, J. P. 1993, MNRAS, 261, L8
Williams, B. F., Ciardullo, R., Durrell, P. R., et al. 2007a, ApJ, 654, 835
Williams, B. F., Ciardullo, R., Durrell, P. R., et al. 2007b, ApJ, 656, 756
Worthey, G., Faber, S. M., & Gonzalez, J. J. 1992, ApJ, 398, 69
Worthey, G., Faber, S. M., González, J. J., & Burstein, D. 1994, ApJS, 94, 687
Wu, X., Gerhrd, O., Naab, T., et al. 2014, MNRAS, 438, 2701
Wu, X., & Tremaine, S. 2006, ApJ, 643, 210
Zabludoff, A. I., Geller, M. J., Huchra, J. P., & Vogeley, M. S. 1993, AJ, 106, 1273
Zabludoff, A. I., Huchra, J. P., & Geller, M. J. 1990, ApJS, 74, 1